NTNU – Trondheim
Norwegian University of
Science and Technology

Laboratory Demonstration of Frequency Support Provision from VSC-HVDC-connected Full Converter Wind Turbines

Jon Nerbø Ødegård

Master of Energy and Environmental Engineering
Submission date: June 2015
Supervisor: Kjetil Uhlen, ELKRAFT

Norwegian University of Science and Technology
Department of Electric Power Engineering

Acknowledgment

I wish to thank my supervisor, Professor Kjetil Uhlen for guiding me in an demanding field of study. By accepting and submitting the proposed problem description, you have motivated me to deliver my best.

For giving me the opportunity to pursue my field of interest, I give my sincere thanks to Kamran Sharifabadi and Atle Rygg Årdal. By contributing as co-supervisors and in preparing the problem description, you have introduced me a field of work I wish to become a part of.

For providing the best study environment anyone can ask for, room G-220 receives endless appropriate applause. Our shared laughs will be missed and I wish the graduates all the best.

Jon Ødegård
2014

Abstract

The state of the art in wind power technology is VSC-HVDC-connected (Voltage Source Converter-High Voltage Direct Current) offshore wind farms of Full Converter Wind Turbines (FCWT). This latest generation of wind power plants provide great opportunities with regard to efficiency and flexibility, but poses new challenges with regard to power system stability, as the asynchronous operation inertially decouples the generators from the residual power system. By utilising the flexibility of VSC-control, the goal is to improve the dynamic behaviour of the power system by coupling the system frequency and generator speed, and hence provide frequency support.

The frequency support control strategies are initially designed by contextualising the wind power plants in classic power system stability theory. By the knowledge of lacking primary control in wind farms, it was predicted that an inertia response would compromise system damping as the turbines *demand* power when returning to nominal speed, whereas classic power plants *provide* power. The effectiveness of the design was evaluated by the results gathered from two experimental methods, simulation and laboratory. The simulation model was constructed in MatLab SimuLink and is a mathematical power flow model. Since the time scope of inertia response is in seconds, the microsecond switching of the converters is not modelled. The laboratory model was constructed by a 17 kW grid and a 55 kW wind farm equivalent connected by 60 and 20 kW VSC-converters. All converters are FPGA-controlled enabled by the graphical programming environment LabView and CAN-bus messages. The system load is pure resistive and the perturbation of the system is changing this resistance.

The auxiliary control structure was designed with simplicity as the key feature. By onshore frequency measurements, the deviation from nominal was scaled and mirrored on to the HVDC-voltage. This was denoted Scaled Deviation Mirroring, SDM. The same technique was used to couple the HVDC-voltage to the offshore frequency, and then couple the offshore frequency to the wind turbine speed. If neglecting any regulation delay, this would allow the wind turbine to swing in phase with the grid frequency. This novice control reduced the frequency drop by 35.3 % and the overshoot by 12.5 %, but the oscillations sustained twice as long.

Using the prediction of compromised damping, a secondary controller was designed with the intention to damp the oscillations. Since the wind turbines lacks primary regulation (governors), regulation of the residual grid must ensure damping for an added inertial mass. Any inertial energy providetp the grid, must therefore be returned. A key characteristic of the full converter wind turbine has already been pointed out - asynchronous frequency - and this is utilised in the Wind Turbine Stabiliser control (WTS-control). Com-

pletely decoupled frequency allows the inertia response to be phase shifted without restriction, and it can be optimised to reduce frequency drop and improve damping. The results showed that a wind turbine frequency response phase lagging $15 - 20°$ significantly improved damping, but on the expense of frequency drop reduction. The addition of WTS-control improved the frequency drop by 29.4 %, the overshoot by 62.5 %, while sustaining the oscillations for 50 % longer compared to the reference.

The fact that a lagged response improves the system performance pave way for two conclusions. Firstly, the regulation does not need to be stressed for optimal performance, as the response is nevertheless lagged on purpose. Component ratings can then be easier met, as high currents are avoided. Secondly, the lag is a proof of the greatest weakness of the wind turbines, no primary regulation. The auxiliary control must then be regarded as a method for improving system interaction, rather than local contribution. The lagging wind turbine inertia response facilitates an effective primary regulation of residual grid by providing inertia reserves at the right time, but also demanding accelerating power at the right time.

Sammendrag

Fremtiden innen vindkraftproduksjon er VSC-HVDC-tilkoblede (Voltage Source Converter-High Voltage Direct Current) offshore vindparker med asynkrone vindturbiner med frekvensomformere. Denne siste generasjons vindkraft gir store muligheter med tanke på effektivitet og fleksibilitet i drift, men gir nye utfordringer når det kommer til stabilitet i kraftsystemene, da asynkron drift kobler treghetsmomentet i turbinene fra resten av nettet. Dette er uheldig da frekvensresponsen som etterfølger en driftsendring er invers proporsjonal med det totale treghetsmomentet. Ved å bruke fleksibiliteten i VSC-omformerkontroll er det ønskelig å forbedre de dynamiske egenskapene til kraftnettet ved å koble systemfrekvensen til generatorhastigheten i vindturbinene, og dermed øke treghetsmomentet i systemet.

Strategien for frekvensstøttekontroll er innledningsvis designet ved å kontekstualisere vindkraftproduksjon i klassisk kraftsystemteori. Ved å bruke kunnskap om manglende primærkontroll i vindkraft, var det forutsett at det ekstra treghetsmomentet fra vindturbinene ville gå på bekostning av dempingen av frekvensresponsen. Grunnen til dette er at all energi som leveres til nettet, må returnere for å bringe vindturbinen tilbake til nominell hastighet. Dette skaper energiflyt fram og tilbake inntil primærreguleringen får dempet det ut. En kontrollstrategi for å forbedre demping ble derfor designet. Kontrollstrategiene ble evaluert ved to eksperimentelle metoder, simulering- og laboratoriemodell. Simuleringsmodellen ble konstruert i MatLab Simulink og er en matematisk kraftflytmodell. Laboratoriemodellen er satt sammen av en 17 kW nett- og 55 kW vindturbinekvivalent, koblet med 60 og 20 kW omformere. Alle omformerne er FPGA-kontrollert muliggjort av det grafiske programmeringplattformen LabView. Systemet ble forstyrret ved å endre en resistiv last.

Tilleggskontrollstrukturen ble designet med enkelhet som målsetning. Ved systemfrekvensmåling ble avviket fra nominell verdi speilet til HVDC-spenningen. Dette er omtalt som SDM (Scaled Mirrored Deviation). Samme struktur ble brukt for å regulere offshore nettfrekvens, ved måling av HVDC-spenning. Vindturbin hastigheten ble så regulert med SDM ved offshore nettfrekvensmåling. Hvis man ser bort fra reguleringsforsinkelser vil vindturbinen da svinge i fase med systemfrekvensen. Denne enkle kontrollstrategien reduserte frekvensfallet med 35,3 %, oversvingning med 12,5 %, men lot svingningene vedvare dobbelt så lenge.

På grunn av de vedvarende svingningene ble vindturbinkontrollen endret for å bidra til å dempe systemet. Siden vindturbinene mangler primærregulering er det resterende nettet, og dets regulatorer, ansvarlig for å stabilisere vindturbinene. Nøkkelen til å muliggjøre demping er den asynkrone driften av vindturbinene. Uten restriksjoner kan vindturbinresponsen faseforskyves,

slik at bidraget kommer til ideell tid. Denne kontrollstrategien omtales som Wind Turbine Stabiliser Control (WTS). Resultatene viste at en vindturbinrespons med $15 - 20\circ$ negativ faseforskyvning forbedret demping, men på bekostning av reduksjon av frekvensfall. Frekvensfallet ble redusert med 29.4 %, oversvingning med 62,5 %, med svingningene vedvarende 50

At en forsinket vindturbinfrekvensrespons forbedrer ytelsen til kraftsystemet forteller to ting. For det første kan man la være å stresse kontrollsystemene unødig, da treget uansett er et ønske. Det er likegyldig om dette skjer i tilleggskontrollstrukturen eller i VSC-kontrollen. Da er det enklere å møte komponentkrav, da høye strømmer kan unngås. For det andre er en forsinket vindturbinrespons en bekreftelse på dens største svakhet, ingen primærregulering. Man kommer ikke vekk fra den viktige rollen til regulatorene i det resterende nettet. Kontrollstrategiene for vindturbinene må dermed ansees som en metode for forbedret systemsamhandling, heller en metode for systembidrag. Den forsinkede responsen legger til rette for effektiv primærregulering ved å bidra med effekt i riktig tid, men også kreve effekt tilbake til riktig tid.

Contents

List of Figures

List of Tables

Chapter 1

Background

The latest generation of wind turbine topologies provides great opportunities with regard to efficiency and flexibility, but poses new challenges with regard to power system stability. Generation interfaced by power electronics interact with the power system in a fundamentally different way than classical generation. In addition, an increasing willingness to place wind farms offshore will require direct current power transfer, as traditional alternating currents transmission is rendered impractical/impossible, due to high charging currents.

Voltage Source Converters (VSC) is the latest advance in converter technology. Semi-conductor components with self commutating capabilities enables high frequency switching at command, making converters able to fully synthesise AC-voltages. Even if some losses are introduced, the advantages has rendered these less important. Individual control of active and reactive power is among those most desirable. For offshore applications, the ability to fully synthesise AC-voltage is a necessity to operate an islanded grid.

Power systems are maintained stable by balancing production and consumption. As for any other mechanical system, any imbalance in power yields an acceleration/deceleration, covering the power deficit by releasing/absorbing kinetic energy. With converter interfaced generation however, the local frequency control prevent any contribution of kinetic energy. High integration of converter interfaced generation is therefore vulnerable to operational disturbances as there are less rotating mass, and hence less energy, to withstand power imbalances. Limitations to frequency deviations are defined by the grid code provided by ENTSO-E [1] and the associated Transmission System Operators local requirements. This includes duration and absolute value. ENTSO-E also provide regulations for HVDC-connections [2].

1.1 System of investigation

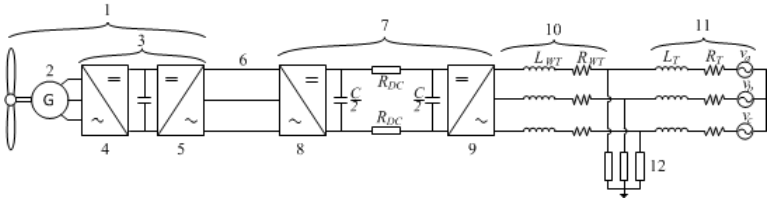

Figure 1.1: System configuration and notation, 1. Wind Turbine, 2. Wind Tubine Generator, 3. Turbine Frequency Converter, 4. Generator Drive Converter, 5. Wind Turbine Grid Converter, 6. Offshore Grid, 7. VSC-HVDC-link, 8. HVDC Offshore Grid Converter, 9. HVDC Onshore Grid Converter, 10. Transmission Line, 11. Onshore Grid, 12. Load

There are a number of wind power plant configurations. A major objective of this report is to realise a realistic configuration. In addition, the system should pose some challenges. Lastly, the system should assess state of the art technology. The chosen topology is therefore an offshore Full Converter Wind Turbine (FCWT) farm connected by Voltage Source Converter High Voltage Direct Current (VSC-HVDC) link to a onshore weak grid. The configuration is illustrated in figure 1.1.

From an engineering point of view, offshore wind is beneficial for stable power supply as winds are more stable, with less turbulence caused by any topological disturbances. The uniform terrain also allows the wind farm to span over greater areas. Offshore wind power plants also represent the more esthetically pleasing solution viewed by the general public. HVDC is the only viable solution for long distance bulk power transmission, as traditional AC or HVAC impose high charging currents. VSCs are necessary since an offshore wind farm needs a synthesised AC grid. The inclusion of HVDC poses a number of challenges, and sets the premise for multiple investigations. These include offshore grid control, coordinated response for frequency support, protection and more.

The wind turbines is chosen to be of full converter topology. This is regarded as the future of wind turbine configurations, as converter technology is rapidly improving. They allow for very flexible operation, which is beneficial both in terms of maximising power and for realising new control strategies. The generator-blade set is the DTU Reference Turbine [3].

1.2 Scope of Work

The scope of work can be summarised by three points.

1. Objectives
    - Main: Improve dynamic behaviour of the system
    - Secondary: Highlight flexibility of VSC-control and gain understanding of wind power plant interaction with classic power systems.
2. Method
    - Contextualise wind power plants in classic stability theory
    - Designing auxiliary VSC-control
    - Test design by simulation and laboratory
3. Challenges
    - Maintain a stable system for all perturbations
    - Maintain component ratings
    - Assessing a realistic configuration

Frequency support from offshore wind by converter control has been studied in various topologies [4], [6], [7] and [5], discussing HVDC control, turbine control, DC-link stored energy and wind torque characteristics respectively. The aim of this thesis is to test a full configuration, where the coordinated control of HVDC and FCWTs is tested, where the speed response and inertia distribution reflect a real world application and the aerodynamic behaviour of the wind turbine is taken in to account. Note that the aerodynamic behaviour is neglected throughout the length of the thesis, only to be brought up in chapter 7.

Chapter 2

Frequency stability

Frequency steady state is achieved when the production and the consumption are balanced, and frequency steady state is therefor the obvious control measure in power regulation. In European power systems the synchronous frequency is 50 Hz, and the power system as a whole should be regulated with this control objective. With power sources ranging from coal and gas to wind and solar, there are a vast number of power plant control possibilities and strategies, but they all share grid operation responsibilities to one degree or an other. Hydro power is traditionally regarded as a great contributor in stabilisation, due to its quickness of water flow regulation. Solar power on the other hand has one main objective, to supply maximum power at any time. The following section aim to highlight the importance of system inertia and power reserves. It will also provide motivation for implementing frequency support from wind power.

2.1 Generation Control and Regulation

2.1.1 Synchronous Generation Characteristics

Considering a system as a sum of power loads and power generation, the swing equation describes system frequency dynamics.

$$M_{eq}\frac{d\omega}{dt} = \sum P_{mech} - \sum P_L, \quad M_{eq} = \frac{2H_{eq}}{\omega_s}, \quad H_{eq} = \frac{\frac{1}{2}J_{eq}\omega^2}{S_n} \tag{2.1}$$

Following the equation 2.1, the frequency must decrease if the load exceeds the generated power and vice versa. The characteristics from figure 2.1 is given for an ideal generator. The dotted line indicates speed power characteristics of the unregulated system [8], ch. 2.3.3. The regulated system is made by speed control, where the input mechanical power is regulated in order to balance load and generation. This is further referred to as governor control. The strategy for governor control is to compensate for system frequency

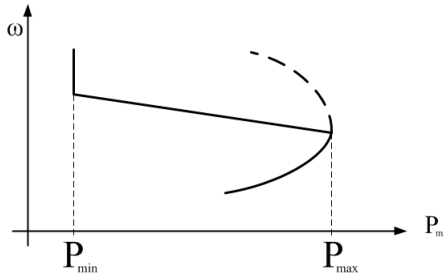

Figure 2.1: Speed-power regulation, Dashed: unregulated and Solid: regulated system

changes. If system frequency drops, the generated power should increase in order to maintain the balance and stabilise the system frequency.

The linear interval can be normalised to obtain the equation for the operation for an arbitrary governor controlled generator. Subscript n indicates nominal operation. The speed droop constant is introduced, ρ_g. This is the factor on which the relation between frequency change and power change can be made. The power droop constant is the inverse, $K_g = \frac{1}{\rho_g}$.

$$\frac{\Delta f_s}{f_n} = -\rho_g \frac{\Delta P_g}{P_n}, \qquad \frac{\Delta P_g}{P_n} = -K_g \frac{\Delta f_s}{f_n} \tag{2.2}$$

2.1.2 Primary Control

Primary control is the coordinated regulation of multiple loads and generators. For a system of N generators, one can make the following relation between total change of load, ΔP_L, and system frequency.

$$\Delta P_L = -\Delta f \sum_{i=1}^{N} \frac{K_{gi}\ P_{ni}}{f_n} \tag{2.3}$$

K_{gi} and P_{ni} indicates the the power droop constant and local nominal power for generator i respectively. Each generator contributes to meet the new power demand. The amount of contribution depends on the droop constant.

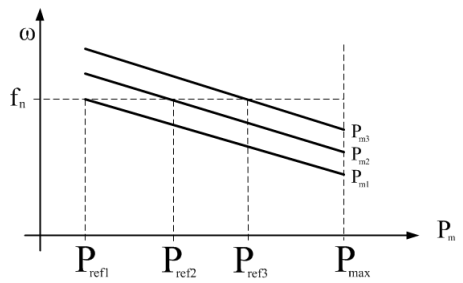

Figure 2.2: Secondary control, shifted speed-power characteristics by nominal power reference.

2.1.3 Secondary Control

Primary control is made with frequency steady state as the ultimate control objective. For a power system the main control objective of all governors is to maintain system frequency at the reference level, 50 Hz. This is classically done by centrally placed operations and manual power reference updates. By a new reference given to one or more governors, the system frequency will reach a new operating point by the new power balance. This is illustrated in figure 2.2

2.1.4 Tertiary control

Tertiary control is operation planning over a longer term. This would include weather forecast (wind, solar, temperature) and market considerations. An other objective of tertiary control is to plan operation so that primary and secondary control can be executed. For example, if all generators is running at maximum power, there is no reserve to compensate a load increase. Spinning reserves is therefore an necessity for power system control. Optimising the dispatch of supportive control is also defined as tertiary control.

2.2 Dynamic Response

The previous sections discussed regulation between steady state operating points without including the dynamic response. When evaluating the dynamic response of a system, two more stages should be introduced, inertia response and rotor swings. This distinguishing is necessary due to the nature of the grid dynamics. Rotor swings are determined by by dynamic behaviour of each of the generators, such as transient impedance and electric closeness

to the disturbance. Inertial response is determined by the power balance of the system. This is not a local response, but rather a system response. The inertial response is acceleration (or deceleration) of rotating mass in order to balance power imbalances by release (or absorption) of rotational energy. Figure 2.3 illustrate a typical frequency response, and a rough classification of the stages.

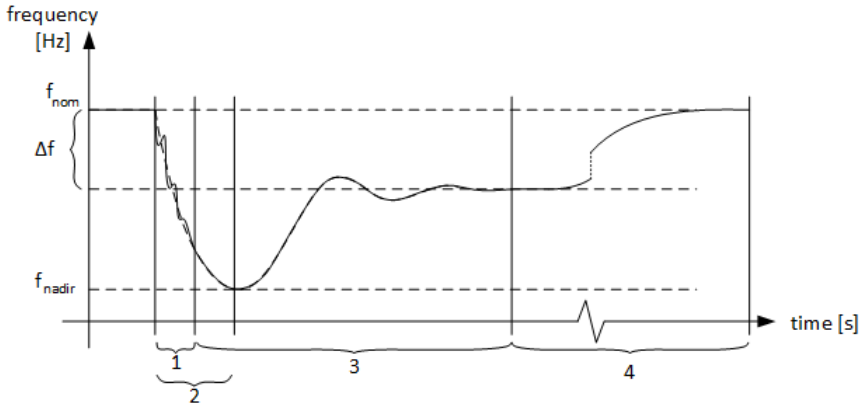

Figure 2.3: Dynamic response of the regulated power system. 1. Rotor Swings 2. Inertia Response 3. Primary Control 4. Secondary Control

2.2.1 Rotor Angle Swings

When evaluating the initial response of the generators, one assume constant mechanical power. That is, the governor have not had time to react to a system operational change. From [8], ch. 9.2, the standard generator dynamic model is used and simplified by assuming constant flux linkage, resulting in equation 2.4.

$$P(\delta_0) = \frac{E^{'}V_s}{x_d^{'}} sin\delta^{'} \tag{2.4}$$

When operational conditions are changed, each generator will change it's power angle characteristics due to the transient impedance in the denominator. The rotor will immediate after the change seek a new stable operation. In this context, stable operation is the balance between locally produced power and mechanical input power. This is illustrated in figure 2.4. P_e^- and P_e^+ is the power-angle curve before and after a operational change.

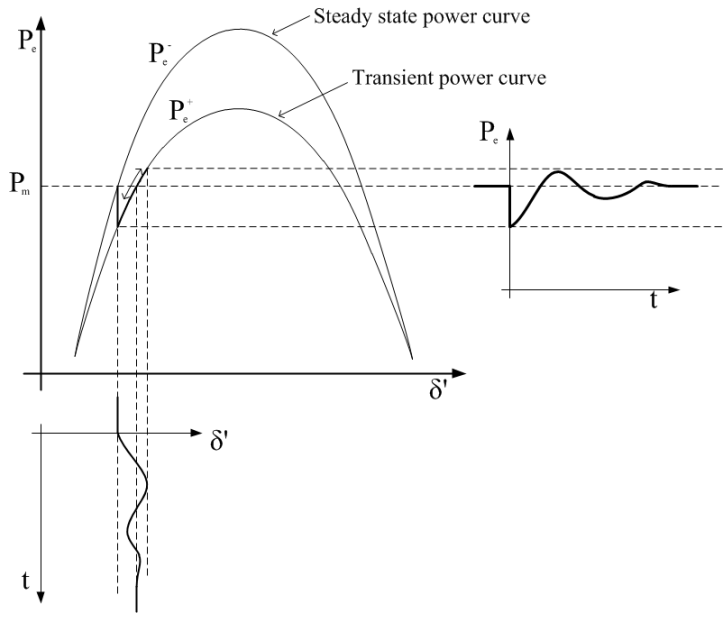

Figure 2.4: Rotor angle response by a operational change

2.2.2 Inertia Response

The rotor swings are invoked by operation change, but does not contribute in covering the power deficit. If rotor swings are neglected there will be constant power output, as mechanical power is constant due to slow acting governors. Slow is a relative term in this context. The term inertia response originates in the energy release (absorption) from acceleration, where energy (and power) is a proportional to inertia ($E = \frac{1}{2} I_{eq} \omega(t)^2$ and $P = \frac{dE}{dt}$).

By the assumption that all generators maintain synchronism through rotor swings, the following relations is valid [8], ch. 9.3,

$$\Delta P_0 \;=\; \sum_{i=0}^{N} \Delta P_i \tag{2.5}$$

$$\frac{d\Delta\omega_1}{dt} \;=\; \frac{d\Delta\omega_2}{dt} \ldots \;=\; \frac{d\Delta\omega_i}{dt} \;=\; \epsilon \tag{2.6}$$

Here, ΔP_0 is the total power released or absorbed from rotational kinetic energy in the system and is equal to the power imbalance. ΔP_i is the power released from generator i and $\Delta\omega_i$ the speed deviation in generator i. Using the swing equation to express ΔP_i as a function of frequency change and inserting in equation 2.5,

$$\Delta P_i \;=\; M_i\epsilon \tag{2.7}$$

$$\Delta P_0 \;=\; \epsilon\sum_{i=0}^{N} M_i \tag{2.8}$$

Rearranging gives the relation,

$$\epsilon \;=\; \frac{\Delta P_0}{\sum\limits_{i=0}^{N} M_i} \tag{2.9}$$

This equation shows that the (de)acceleration of the system is inversely proportional to the total inertial reserves in the system. From this point inertial reserves is referred to as this sum of generator inertia.

2.2.3 Primary Response Dynamics

The initial response of the system invokes governor regulation of mechanical power in order to cover the power load difference, ΔP_0. The system is then regulated by the characteristics from figure 2.1 by rotor speed measurements. Due to the droop of the speed-power characteristics, the steady state frequency will be shifted after a power disturbance. As mentioned, a system of generators have a coordinated response in order to properly regulate. Also, large systems may have electrically separated areas which may work against each other, this can be evaluated and detected by modal analysis.

2.3 Next Generation Power System Components

2.3.1 Primary Regulation of Wind Turbines

A key difference between conventional power generation and wind plants are the mechanical power input. Obviously, wind turbines are driven by an external force which is uncontrollable. As maximum power from the wind turbine is the main control objective, there are no power reserve, and consequently no primary control. Power systems with high share of wind power is therefore vulnerable for faults. Tertiary control must be done with care in order to secure power reserves elsewhere in the system.

2.3.2 Asynchronous Generation Inertia Response

Firstly, a synchronous wind turbine is discussed. It is made a preliminary assumption that the input mechanical power is constant. In other words, the aerodynamic effects are neglected. Equation 2.7 is then equally valid. The inertia constant is a function of the blades, shaft, gearbox and rotor, which all have high mass. In addition, the blades are far from center of mass, which from the generic inertia equation, $J = \int \rho(r, \phi, l) r^2 dV$, yields high inertia. A synchronous generator will then provide inertial support like any other generator.

The full converter wind turbine configuration has many advantages with regard to power maximisation during steady state operation (variable speed), but there are a major trade off with regard to inertial response. For any variation of frequency on the grid side, there are no variation on generator side, due to fast regulation of converters and local frequency references. In other words, from the grid side the power supplied from the wind turbine is perceived constant at any time varying system frequency. Then, equation 2.8 yields that there are zero inertia in the FCWT. If equation 2.8 is reviewed from the generator side, the frequency is constant. But lets assume that the generator side frequency is time varying. Then the wind turbine will follow equation 2.9. The conclusion is that FCWT has inertia response only if generator frequency is changed. When auxiliary controls for inertia support are designed, this local frequency control can be used to produce a frequency response.

2.3.3 Inertial Reserves in Power Electronics

Discussing inertial reserves in power electronic components may not make sense as there are no rotating parts and hence no inertia. This discussion is though necessary due to the way power electronics interact with the grid. The frequency response is invoked by the power imbalance, and since the only energy storage in classical power systems is the rotating generators, inertial reserves is the generic term. Frequency containment reserves is more descriptive when including the new power system components, since these also have energy storing capabilities. The capacitances found in power electronics and DC-links are energy storages. Energy stored in a capacitor is given by $E_c = \frac{1}{2}CV^2$. The time derivative is per definition power. Since the capacitance is a constant value, power output must be invoked by time varying voltage.

Chapter 3

VSC Control

The use of Voltage Source Converters, VSC, in wind power grid connection has been presented shortly. A full description of VSC-HVDC advantages is found in [9]. The following chapter aim to highlight control flexibility and to present the classical control strategies. By doing so, auxiliary control strategies can be designed with analytical derived predictions.

3.1 Modelling of VSC

Investigating the behaviour of VSCs can be done in various degrees of detail. The decisive parameter when a dynamic model is chosen, is the scope of time. Investigating switching and harmonics obviously requires very fine computational intervals as the semiconductors is operating at several thousand hertz (less than millisecond intervals). From chapter 2 inertial response are recognised as the dynamics spanning from a few milliseconds to seconds after a operational disturbance. The high frequency switching is not interesting in this context. Differences between VSC technologies can then be neglected, as these aim to improve switching schemes and harmonic content. The following sections explains the average model, clarifies punctuation and present tuning strategies.

Figure 3.1 shows a basic grid connected two level VSC. By a pre-specified switching scheme which synthesise an AC-voltage at a given frequency and phase angle, it can supply/receive power to/from the DC side depending on the current sign (in this case positive DC-current yields rectifier mode). The transition from inverter to rectifier mode of operation can be made seamlessly. The voltage equation known for such a converter is found in [10] and given by equation 3.1.

$$V_{a,b,c\ rms} = \frac{m_a\ V_{DC}}{2\sqrt{2}} \tag{3.1}$$

Using the relation in equation 3.1, figure 3.1 can be reduced to figure 3.2. This is justified by the aforementioned neglection of harmonics on AC side and by assuming no power loss in the converter. The two circuits are linked

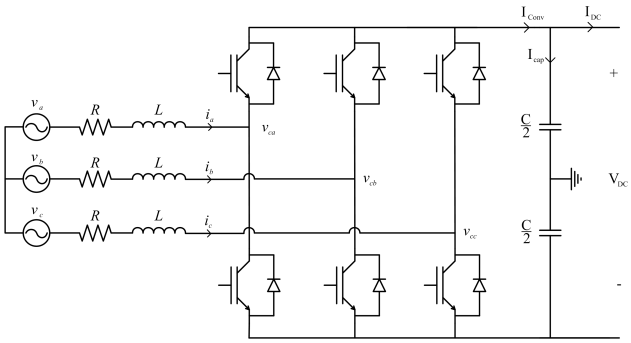

Figure 3.1: Grid connected two level Voltage Source Converter

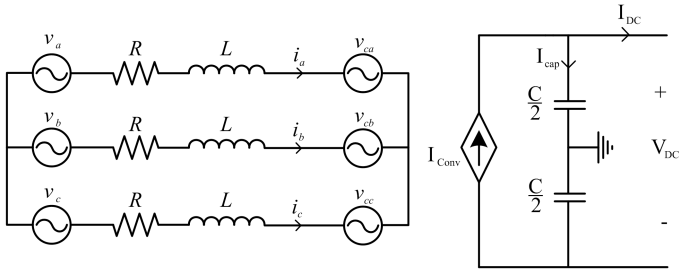

Figure 3.2: VSC reduced by average model

by the relation $P_{AC} = P_{DC}$. The current is then found by the following relation.

$$3V_{a,rms}I_{a,rms} = V_{DC}\ I_{DC} \tag{3.2}$$

$$I_{DC} = \frac{3I_{a,rms}m_a}{2\sqrt{2}} \tag{3.3}$$

With the average model established, the scoped simulation work can be done by a significantly more analytical method. This saves computational time and makes results more interpretable as non-influential parameters can be left out.

VSC control is generally recognised as power flow management. On either terminal, AC or DC, an amount of power is supplied or demanded, and the control must operate in such a way that these requirements are fulfilled,

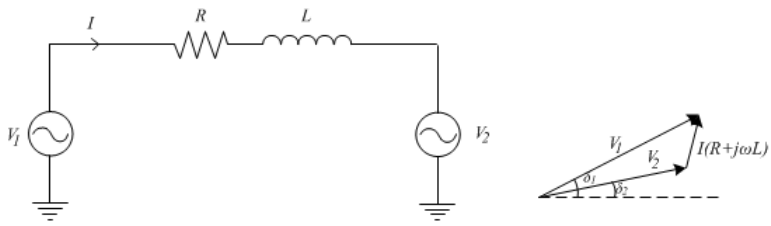

Figure 3.3: a) Transmission line equivalent b) Phasor diagram

while maintaining component ratings. Figure 3.3 and equations is known from classic power flow analysis. G is the real part, while B is the imaginary part of the admittance matrix Y. Details is found in [11], ch. 6.4.

$$P_1 = -\sum_{k=1}^{2} |V_s||V_r|(G_{1k}cos(\theta_{1k}) + B_{1k}sin(\theta_{1k})) \tag{3.4}$$

$$P_2 = -\sum_{k=1}^{2} |V_s||V_r|(G_{2k}cos(\theta_{2k}) + B_{2k}sin(\theta_{2k})) \tag{3.5}$$

$$Q_1 = -\sum_{k=1}^{2} |V_s||V_r|(G_{1k}sin(\theta_{1k}) + B_{1k}cos(\theta_{1k})) \tag{3.6}$$

$$Q_2 = -\sum_{k=1}^{2} |V_s||V_r|((G_{2k}sin(\theta_{2k}) + B_{2k}cos(\theta_{2k})) \tag{3.7}$$

Comparing figure 3.3 to figure 3.2, the line equivalent is recognised. Since the converter voltage is controlled in both phase angle and magnitude, it can produce or deliver the desired active and reactive power.

3.1.1 Utilizing $dq-$reference frame in VSC control

The suitable method of VSC control is by vector control. The basic principle is to use the Park-transformation in order to decompose the current and voltage in two rotating components, d and q, which individually controls active and reactive power. Further details regarding this transformation and it's benefits in VSC control can be found in [12, 13]. The basic steps is covered in the following paragraphs.

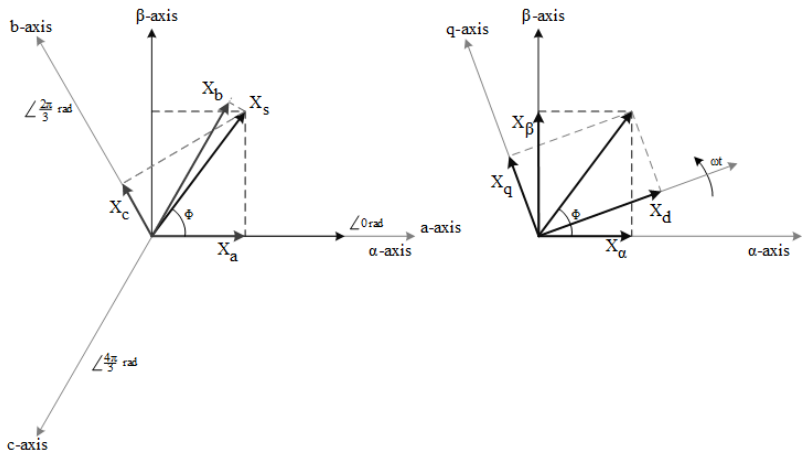

Figure 3.4: Projection of space vectors Left: abc- to $\alpha\beta$-axes Right: $\alpha\beta$ to dq-axes

The Park-transformation serves the purpose of transforming abc-components into $dq-$components directly. By introduction of space vector theory [13], all the three phase quantities can be expressed as one virtual vector in space. The $\alpha\beta$-axes is introduced as reference. This is in essence an imaginary plane in which voltage and current space vectors is expressed as phase shifted rotating quantities.

Figure 3.4 shows an arbitrary space vector with it's corresponding symmetric abc-components. $\alpha\beta$-axes is indicated as orthogonal axes with α-axis parallel to a-axis. The projections to $\alpha\beta$-axes is then calculated by trigonometric identities.

$$\vec{X_s} = X_a\ sin(\omega t)\ e^{j0} + X_b\ sin(\omega t + \frac{2\pi}{3})\ e^{j\frac{2\pi}{3}}\ X_b\ sin(\omega t + \frac{4\pi}{3})\ e^{j\frac{4\pi}{3}} \quad (3.8)$$

$$\begin{aligned}\vec{X_s} = X_a\ sin(\omega t) &+ X_b\ sin(\omega t + \frac{2\pi}{3})\ (\ cos(\frac{2\pi}{3}) + jsin(\frac{2\pi}{3})\ ) \\ &+ X_c\ sin(\omega t + \frac{4\pi}{3})\ (\ cos(\frac{4\pi}{3}) + jsin(\frac{4\pi}{3})\ )\end{aligned} \quad (3.9)$$

In a balanced system, $X_a\angle 0° = X_b\angle 120° = X_c\angle 240°$, the space vector will have constant length in $\alpha\beta$-coordinates. Note that the quantities is given in peak value.

$$\vec{X_{\alpha\beta}} = \frac{3}{2} X_a e^{j\phi+\omega t} \tag{3.10}$$

Equating real and imaginary values from equation 3.9 gives $\vec{V_s}$ in terms of $\alpha\beta$ coordinates. The constant k is explained later:

$$\begin{bmatrix} X_\alpha \\ X_\beta \end{bmatrix} = k \begin{bmatrix} 1 & -\frac{1}{2} & -\frac{1}{2} \\ 0 & \frac{\sqrt{3}}{2} & -\frac{\sqrt{3}}{2} \end{bmatrix} \begin{bmatrix} X_a \\ X_b \\ X_c \end{bmatrix} \tag{3.11}$$

Now, assuming that $\vec{X_s}$ is rotating with a given frequency in the $\alpha\beta$-reference frame. It is then desired for $dq-$axes to be an orthogonal rotating reference frame at the same frequency. If so, $\vec{X}_s^d$ appears to be stationary, since $\angle\vec{X}_s^d = \angle\vec{X}_s^\alpha + \angle\vec{X}_\alpha^d = \angle\vec{X}_s^\alpha - \angle\vec{X}_d^\alpha = \omega t+\theta-\omega t = \theta$. Equation 3.11 is recognised to be an expression for a stationary orthogonal reference frame. Then, by multiplying it by the rotational matrix we have the desired expression.

$$R = \begin{bmatrix} cos(\omega t) & -sin(\omega t) \\ sin(\omega t) & cos(\omega t) \end{bmatrix} \tag{3.12}$$

$$\begin{bmatrix} X_d \\ X_q \end{bmatrix} = k \begin{bmatrix} cos(\omega t) & cos(\omega t - \frac{\sqrt{3}}{2}) & cos(\omega t - \frac{\sqrt{3}}{2}) \\ -sin(\omega t) & -sin(\omega t - \frac{\sqrt{3}}{2}) & -sin(\omega t - \frac{\sqrt{3}}{2}) \end{bmatrix} \begin{bmatrix} X_a \\ X_b \\ X_c \end{bmatrix} \tag{3.13}$$

At any given time, space vectors can be expressed by $dq-$components if the angle (ωt) is known. The typical notation for the $dq-$vector vector and its components is,

$$\vec{X_{dq}} = [X_d + jX_q] \tag{3.14}$$

With space vector transform introduced for an arbitrary vector quantity, its advantages in VSC control should be highlighted. Using equation 3.14 for voltage and current space vectors,

$$\vec{V_{dq}} = [v_d + jv_q] = k\frac{3}{2} V_a e^{j\theta} \quad \vec{I_{dq}} = [i_d + ji_q] = k\frac{3}{2} I_a e^{j\phi} \tag{3.15}$$

The constant k can be chosen to make further calculations more practical. Choosing $k = \frac{2}{3}$ makes the transformation voltage invariant, while choosing $k = \sqrt{\frac{2}{3}}$ makes the power invariant. Invariance implies that numerical values

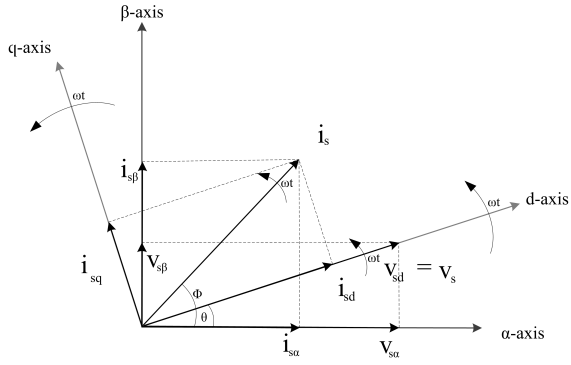

Figure 3.5: Rotating axes transform

can be directly transferred between reference frames. For this configuration the voltage is chosen to be invariant.

$$\vec{V_{dq}} = k\frac{3}{2}V_a e^{j(\omega t+\theta)} \quad \vec{I_{dq}} = k\frac{3}{2}I_a e^{j(\omega t+\phi)} \tag{3.16}$$

When $k = \frac{2}{3}$.

$$S_{dq} = \vec{V_{dq}}\vec{I^*_{dq}} = k^2\frac{3^2}{2^2}V_a e^{j(\omega t+\theta)}\ I_a e^{-j(\omega t+\phi)} = V_a\ I_a\ e^{j(\theta-\phi)} \tag{3.17}$$

Comparing to three phase power from abc-coordinates. Note that V_a and I_a are the peak values.

$$S_{abc} = \frac{3}{2}\vec{V_a}\vec{I^*_a} \tag{3.18}$$

$$S_{abc} = \frac{3}{2}S_{dq} \tag{3.19}$$

A common choice of d-axis reference angle is parallel to voltage space vector. Then $v_q = 0$ reducing the expressions to,

$$S_{abc} = \frac{3}{2}S_{dq} = \vec{V_{dq}}\vec{I^*_{dq}} = \frac{3}{2}\left[(v_d + jv_q)(i_d - ji_q)\right] = \frac{3}{2}(v_d i_d - j\ v_d i_q) \tag{3.20}$$

$$P_{dq} = \frac{3}{2}v_d i_d \qquad Q_{dq} = -\frac{3}{2}v_d i_q \tag{3.21}$$

Then, active and reactive power is controlled individually by i_d and i_q.

3.1.2 Model using $dq-$transformation

Given the power system in figure 3.2, any three phase quantity is expressed in $dq-$components at any given time by measurements. The necessary values needed is then three phase current and three phase voltage, in addition to phase angle. The phase angle measurement is an important part of the control and will be discussed sperately. For now, the voltage angle is assumed to be measured perfectly. As mentioned, the $dq-$vectors appear to be stationary referred to d-axis. The values is then expressed as phasors, and all normal phasor calculus is valid in $dq-$reference frame. The power system equations of figure 3.2 should then be expressed in such a way.

$$v_{a,b,c} \;=\; Ri_{a,b,c} \;+\; L\frac{di_{a,b,c}}{dt} + v_{ca,cb,cc} \tag{3.22}$$

Which by space vector theory equals:

$$\vec{v}_s^{\alpha} \;=\; R\vec{i}_s^{\alpha} \;+\; L\frac{d\vec{i}_s^{\alpha}}{dt} + \vec{v}_{cs}^{\alpha} \tag{3.23}$$

To refer the space vectors to dq-reference frame, the rotational relation between α- and d-axes, $\vec{X}_s \;=\; X_{\alpha\beta} \;=\; X_{dq}\;\vec{X}_{\alpha}^{d} \;=\; X_{dq}\;e^{j\omega t}$ is used.

$$\vec{V}_{dq}e^{j\omega t} \;=\; R\vec{I}_{dq}e^{j\omega t} \;+\; L\frac{d\vec{I}_{dq}e^{j\omega t}}{dt} + \vec{V}_{c,dq}e^{j\omega t} \tag{3.24}$$

Use of product rule on the derivative term:

$$\vec{V}_{dq}e^{j\omega t} \;=\; R\vec{I}_{dq}e^{j\omega t} \;+\; j\omega L\vec{I}_{dq}e^{j\omega t} \;+\; Le^{j\omega t}\frac{d\vec{I}_{dq}}{dt} + \vec{V}_{c,dq}e^{j\omega t} \tag{3.25}$$

The decomposing of the space vector referred to $dq-$axes and rearranging the 3.25:

$$\vec{v}_{dq} \;=\; \begin{bmatrix} v_d \\ v_q \end{bmatrix} \qquad \vec{I}_{dq} \;=\; \begin{bmatrix} i_d \\ i_q \end{bmatrix} \tag{3.26}$$

$$L\frac{d}{dt}\begin{bmatrix} i_d \\ i_q \end{bmatrix} \;=\; \begin{bmatrix} v_d \\ v_q \end{bmatrix} - \begin{bmatrix} v_{cd} \\ v_{cq} \end{bmatrix} - R\begin{bmatrix} i_d \\ i_q \end{bmatrix} - \omega L\begin{bmatrix} 0 & 1 \\ -1 & 0 \end{bmatrix}\begin{bmatrix} i_d \\ i_q \end{bmatrix} \tag{3.27}$$

This equation set will be the basis for control design covered in the upcoming section.

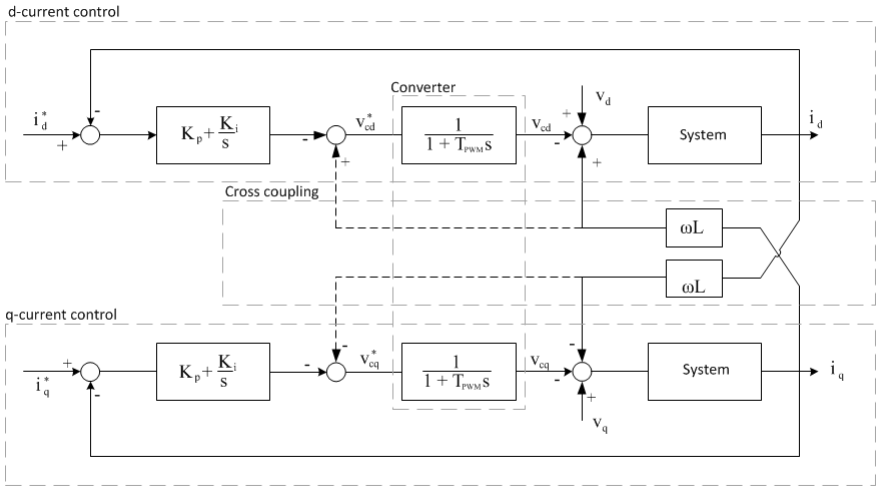

Figure 3.6: Controlled system by $dq-$transformation

3.2 VSC dq-Control

3.2.1 Inner and Outer Control Loops

With the $dq-$transform defined, the VSC can be modeled as a controlled system. The voltage can be regulated, and the current controlled. The regulation of voltage is represented by a delay, T_{PWM}. The details is found in 3.2.3. Using 3.27 and transforming to Laplace domain, equations 3.28 and 3.29 is derived. The block diagram describing the system is given by figure 3.6.

$$sLi_d = v_d - v_{cd} - Ri_d + \omega Li_q \tag{3.28}$$

$$sLi_q = v_q - v_{cq} - Ri_q - \omega Li_d \tag{3.29}$$

The current is PI-controlled. By the double reference input, it is desirable to decouple the system by adding a feed forward loop. These are marked as dashed lines. Without feed forward terms, the system will produce a converter voltage according to this term,

$$V_{cd,cq} = (i^*_{d,q} - i_{d,q}) \left(K_p + \frac{K_i}{s} \right) \frac{1}{1 + T_{PWM} s} \tag{3.30}$$

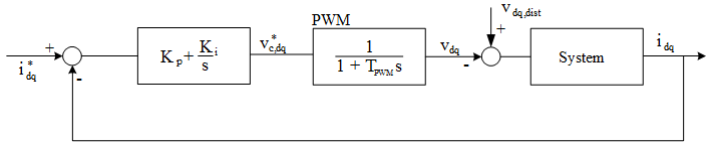

Figure 3.7: Reduced current controlled system by $dq-$transformation

We want equations 3.28 and 3.29 to be independent of each other. The coupling terms is added to the converter reference with opposite sign.

$$V'_{cd,cq} = \left[(i^*_{d,q} - i_{d,q})\left(K_p + \frac{K_i}{s}\right) \mp \omega L i_{q,d}\right] \frac{1}{1+T_{PWM}s} \mp \omega L i_{q,d} = V_{cd,cq} \mp \omega L i_{q,d} \tag{3.31}$$

Inserting in equations 3.28 and 3.29,

$$sLi_d = v_d - v_{cd} - Ri_d + \omega L i_q (1 - \frac{1}{1+T_{PWM}s}) \tag{3.32}$$

$$sLi_q = v_q - v_{cq} - Ri_q - \omega L i_d (1 - \frac{1}{1+T_{PWM}s}) \tag{3.33}$$

Since T_{PWM} is very small, the cross coupling can be then be neglected. The block diagram can then be reduced to figure 3.7.

This is further described as inner control loop in the total cascaded control system. The inner control loop should always be the fastest regulated loop in a system and it does the fine tuning of the system. Since there is many possible disturbances in an electrical system, it is beneficial for quick regulated system to take care of those less important, while the outer control loop manages the ultimate control objective. This could be active power or DC-voltage. The outer control loop is a cascaded controller. A reference is compared and regulated, producing a $dq-$current reference, used by inner control loop. With the complete system described by equations and control blocks, the full control scheme for a VSC can be presented, figure 3.8.

3.2.2 Phase Lock Loop

The phase lock loop, PLL, is a critical controller in the system. The measurement of phase angle and frequency is used in both $dq-$transformation and in generation of gate signals for the converter. However, optimising PLL

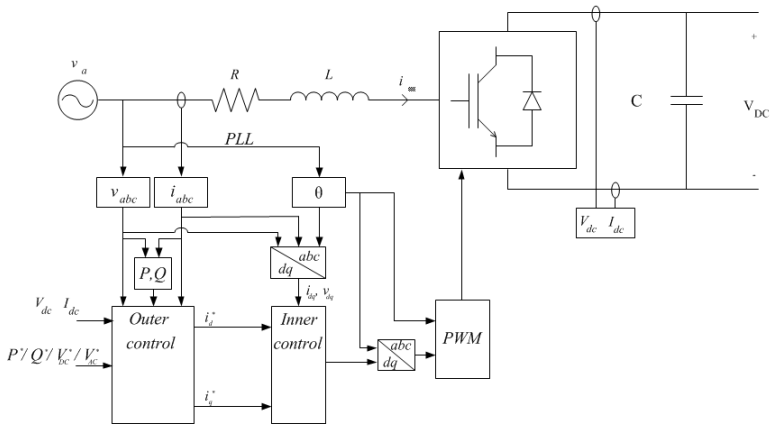

Figure 3.8: VSC-control system

controllers is a field of study on its own and therefore the effect of non ideal PLL is neglected until further notice.

3.2.3 Pulse Width Modulation

The sinusoidal synthesising techniques depends on the topology of the converter and strategy, but the idea is always the same. By controlling the gate signals of the converter a sinusoidal voltage is synthesised on the AC side by high frequency switching. The type of topology chosen determines the harmonic content of the synthesised voltage, but as argued earlier, this is not a part of this investigation. Common PWM techniques include Space-Vector PWM (SV-PWM) and carrier function comparing. Details can be found in [10, 12].

No matter which modulation technique used, a time delay is introduced. This is modeled by a simple first order transfer function. In order to illustrate this, the carrier comparing method is chosen, shown in figure 3.9.

When a new reference is given, that is $V_{control}$ is shifted, the next switching action will happen maximum half a switching period later, as the switching frequency is defined as control signal frequency. We therefore choose $T_{PWM} = \frac{T_s}{2}$.

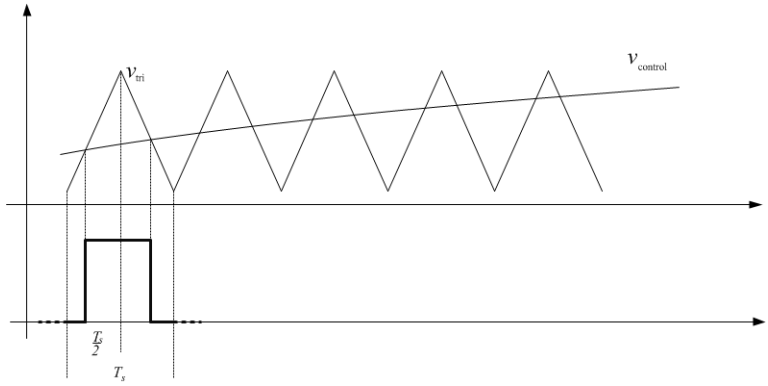

Figure 3.9: Pulse Width Modulation Time Delay

3.3 Tuning

Each VSC will contain one inner and one outer control loop. Referring to figure 1.1, there are 4 converters in the configuration, and therefore 8 controllers. It is beneficial to use specific tuning techniques for certain loops, as they impose specific challenges. These will be controlled using different objectives. All converters have a current inner loop, all of which is desired to operate as quickly as possible. Tuning of outer loops with DC voltage and speed will be presented. The techniques used is widely covered in [14] and the main elements is given in this section. Note that generic notation is used. The loops represent an arbitrary VSC.

3.3.1 Current Control

The tuning technique used for current control is modulus optimum. Investigating figure 3.7 the system needs a mathematical description. Using the voltage balance on AC-side from figure 3.2.

$$v_{dq} - v_{c,dq} = sLi_{dq} + Ri_{dq} \tag{3.34}$$

$$\frac{i_{dq}(s)}{v_{dq}(s) - v_{c,dq}(s)} = \frac{1}{R + sL} = \frac{1}{R}\,\frac{1}{1 + \tau s} \quad \tau = \frac{L}{R} \tag{3.35}$$

The open loop transfer function is then,

$$H_{O.L.,current} = K_p \left(\frac{1 + T_i s}{T_i s} \right) \frac{1}{1 + T_{PWM}} \frac{1}{R} \frac{1}{1 + \tau s} \tag{3.36}$$

Using modulus optimum gives the following relations.

$$T_i = \tau \tag{3.37}$$

This cancels the pole with slower response time, contributing to the quickness of the controller. By use of pole canceling the closed loop transfer function becomes,

$$H_{C.L.,current} = \frac{K_p / \tau R T_{PWM}}{s^2 + \frac{s}{T_{PWM}} + \frac{K_p}{\tau R T_{PWM}}} \tag{3.38}$$

Converting to a known form,

$$H_{C.L.,current} = \frac{1}{s^2 + 2\zeta\omega_n s + \omega_n^2} \tag{3.39}$$

Using the conditions $|H_{O.L.,current}| = 1$ and critical damping factor $\zeta = \frac{1}{\sqrt{2}}$ gives the optimised overshoot. The PI gain is then found to,

$$K_p = \frac{\tau R}{2 T_{PWM}} \tag{3.40}$$

In order to simplify the system when tuning outer control loops, it is desired to simplify the current controller to be a first order transfer function. Using the general form for first and second order transfer functions and integrate the error of a step response, the final value theorem ($t = \infty \Rightarrow s = 0$) approximate the time constant of the first order equivalent. Given the general form of the transfer functions,

$$H_{2.order}(s) = \frac{1}{T_a^2 s^2 + 2 T_a s + 1} \qquad H_{1.order}(s) = \frac{1}{T_{eq} s + 1} \tag{3.41}$$

Equating error yields,

$$T_{eq} = 2 T_a \tag{3.42}$$

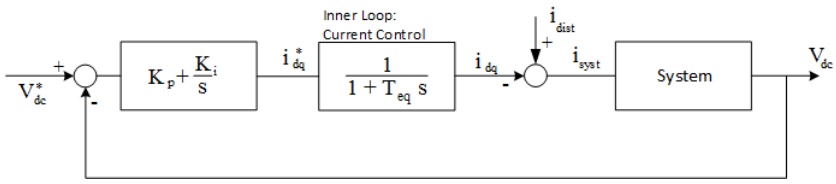

Figure 3.10: Voltage control loop

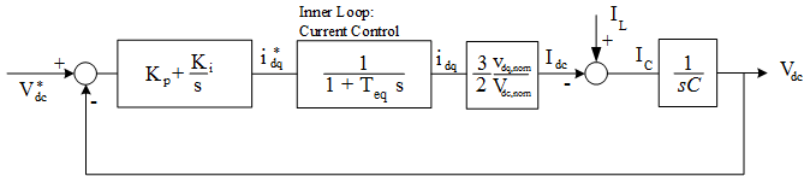

Figure 3.11: Voltage control loop with system equations

3.3.2 DC-Voltage Control

Figure 3.8 shows voltage control to be the outer loop, which simplified is given by figure 3.10. [14] also covers the derivation of a tuned control loop for this configuration. The system transfer function is derived from the current balance in the DC-link.

$$C\frac{dV_{cd}}{dt} = I_{dc} - I_L \tag{3.43}$$

Use of power balance and linearisation by Taylor-series, the following raltion is valid,

$$\frac{\Delta V_{dc}(s)}{\Delta i_d(s)} = \frac{3}{2}\,\frac{V_{d,rated}}{V_{dc,rated}}\,\frac{1}{sC} \tag{3.44}$$

I_L is the load current and is regarded as a disturbance. Including the calculations in the block diagram gives,

The outer loop transfer function is given by equation 3.45. The loop will contain two pure integrators. Using modulus optimum for such a system will cancel the only remaining pole, making the system fundamentally unstable as the phase angle will be at a constant -180. Symmetrical optimum is the preferred method of tuning.

$$H_{O.L.,DCvoltage} = K_{ii}\frac{1+T_{ii}s}{T_{ii}s}\frac{1}{1+T_{eq}}\frac{1}{Cs} \tag{3.45}$$

The crossover angle of 3.45 is expressed by 3.46 and derived to express the relation between crossover frequency and regulato time constant by finding the maximum phase angle. By reinserting the found expression in 3.46, T_{ii} can be related directly to phase margin, ϕ_m. The criteria for regulator time constant is given by equation 3.51.

$$\angle H_{O.L.,DCvoltage}|_{s=j\omega_c} = tan^{-1}(T_{ii}\omega_c) - tan^{-1}(T_{d2}\omega_c) - 180 \tag{3.46}$$

$$\phi_m = tan^{-1}(T_{ii}\omega_c) - tan^{-1}(T_{d2}\omega_c) \tag{3.47}$$

$$\frac{\delta\phi_m}{\delta\omega_c} = \frac{T_{ii}}{1+T_{ii}^2\omega_c^2} - \frac{T_{eq}}{1+T_{eq}^2\omega_c^2} = 0 \tag{3.48}$$

$$\omega_c = \frac{1}{\sqrt{T_{eq}T_{ii}}} \tag{3.49}$$

Then 3.49 inserted in 3.47.

$$T_{ii} = T_{eq}\left(\frac{1+sin(\phi_c)}{1-sin(\phi_c)}\right) \tag{3.50}$$

$$T_{ii} = T_{eq}a^2 \quad where \quad a^2 = \frac{1+sin(\phi_c)}{1-sin(\phi_c)} \tag{3.51}$$

The symmetric optimum criteria for regulator gain, can then be calculated by inserting 3.51 in 3.45, and using the condition $|H_{O.L.,current}| = 1$ gives.

$$K_{ii} = \frac{T_c}{\sqrt{T_{eq}T_{ii}}} = \frac{T_c}{aT_{eq}} \tag{3.52}$$

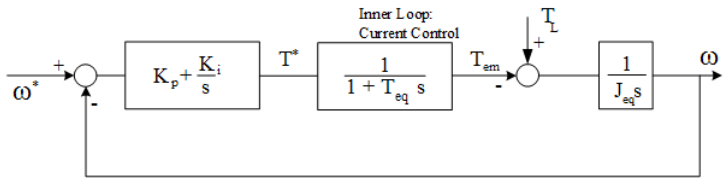

Figure 3.12: Speed control loop

3.3.3 Speed Control

The system equation describing the speed control response is the swing equation.

$$J_{eq}\frac{d\omega}{dt} = T_L - T_{em} \tag{3.53}$$

As the system equation is also a pure integrating differential equation, it matches the capacitance equation of DC-link in form, therefore symmetric optimum is also applicable for this system.

Chapter 4

Control Strategies

4.1 Power Flow Control in VSC-HVDC

Implementation of VSC-HVDC controllers in direct connection with wind power can be done by power-voltage (P-V) characteristics. This implies that one terminal controls voltage and one maintains constant power flow. This is referred as a master-slave configuration, where the voltage controlled converter is denoted as master. This method of power flow management is widely covered in [15].

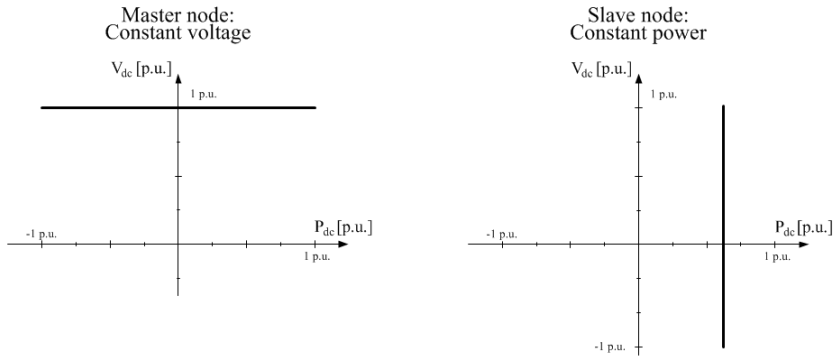

Figure 4.1: Power-voltage characteristics of HVDC-control

Referring to the system sketched in figure 1.1, the control objectives of each converter should be set. With a Full Converter Wind Turbine, FCWT, variable frequency on the generator side enables optimal power output by variable speed. The generator side should then be a generator drive, controlling speed. This implies maintaining the electric torque by current control and voltage regulation. It is known from swing equation that speed is maintained by the balance between electric torque and mechanical torque. With one terminal being a constant power node, the grid side of the turbine converter should be a voltage node.

The offshore grid is completely decoupled from any synchronous machines, it is therefore necessary for the offshore VSC-HVDC-converter to synthesise an AC-voltage. This can be done at an arbitrary frequency. By giving a voltage and frequency reference directly to the PWM-signal generator the frequency can be altered by choice. This is indicated in figure 4.2. This control principle would however not be a viable control in a real world application, as there are no current control putting the converter in risk of very high currents during a fault either on DC- or AC-side. A more robust controller would therefore be a point of investigation if the system were to be realised. On the other hand, it should be noted that there are a lot of freedom in control of the offshore frequency since there are no mechanical- or (almost) no electrical system behaviour to account for. The onshore side of the HVDC-link would be the master node, controlling the DC-voltage. Figure 4.2 present the regulated system by the main control objectives of each converter.

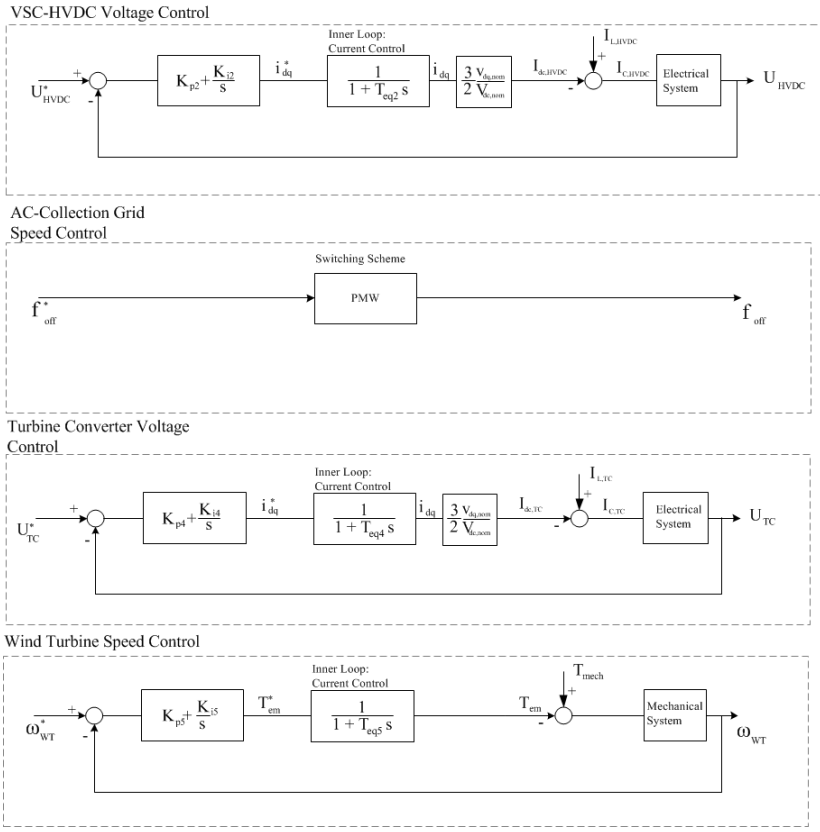

Figure 4.2: Control Scheme of classic VSC-HVDC connected offshore wind installation

4.1.1 Auxiliary Control Principle

The inertial response is release of energy from inertial reserves, as discussed in chapter 2. Classic VSC-HVDC connected power plants was proven inertially decoupled by the discussion in section 2.3, and the non-classical VSC-HVDC presented in this thesis should therefore be coupled. FCWT inertial response would be achieved if there was a local frequency response. The goal of the auxiliary control is then to couple the frequencies on either side.

The HVDC-onshore converter is voltage controlled and synchronised with the grid. For control purposes, the converter does PLL-measurements in order to synchronise the voltage with grid frequency. It is desired to use the PLL-measurement in order to couple grid frequency with DC-voltage. By regulating the HVDC-voltage as a function of onshore frequency measurement, the grid and the HVDC-link is per definition coupled. The offshore frequency reference can similarly be a function of DC-voltage measurements.

The turbine converter has two converters sitting back-to-back, and the grid side does PLL-measurements. Since the converters are physically next to each other, the generator side has direct access to this measurement. The generator speed reference is then regulated as a function of offshore frequency.

The principal control scheme of frequency support viewed in figure 4.3. Each step of the coupling process must be tuned and filtered in order to maintain system stability and component ratings. This is illustrated by a process block.

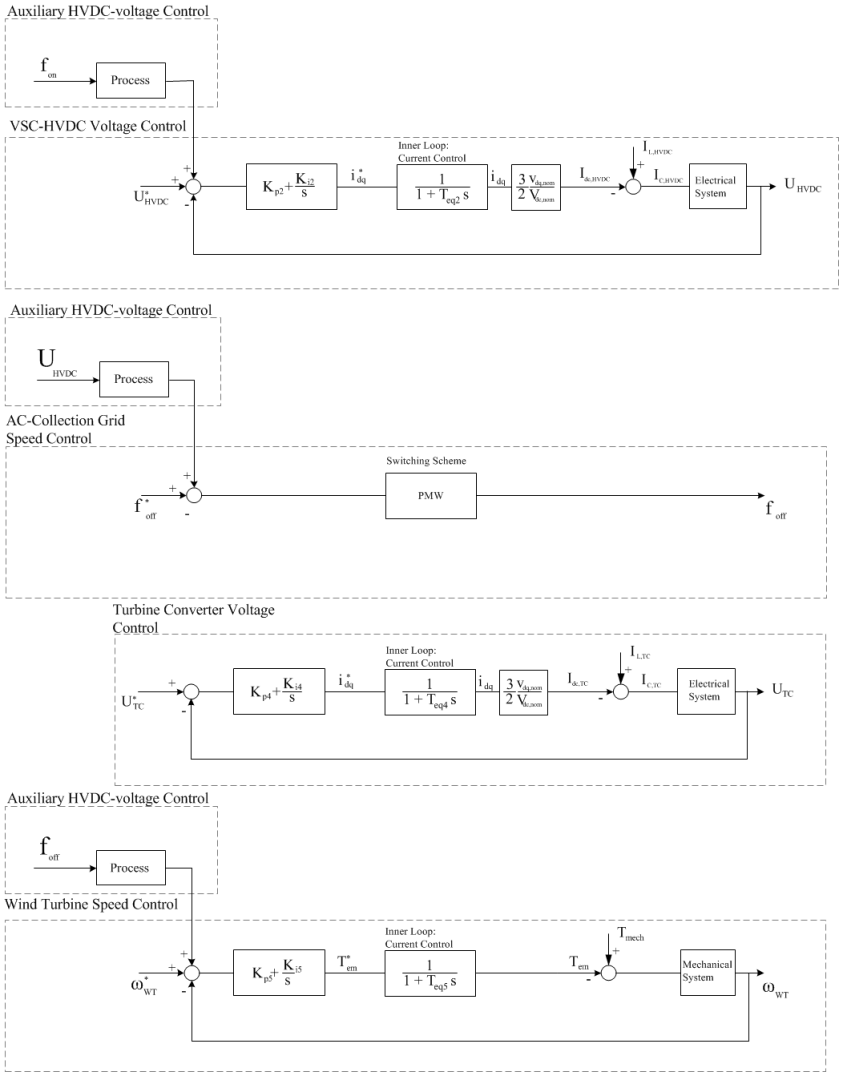

Figure 4.3: Control Scheme of VSC-HVDC connected wind installation with auxiliary control.

4.2 Auxiliary Control Design

When designing the controls for the frequency support, there are a few things that must be kept in mind.

- Energy can be absorbed or supplied by change of rotor speed
- Energy can be absorbed or supplied from the DC-capacitances
- The Wind turbine must return to its initial rotational speed
- There are limits to rotational speed drop of the wind turbine
- There are limits to voltages in HVDC link

To repeat, the main objective of the frequency support controls is to make the system perform better under disturbances. Until this point this has been synonymous with higher inertia reserves, which from equation 2.9 gives a reduce acceleration. This is a modified truth, because there are two characteristics of frequency response which is associated with stability, oscillation amplitude and damping.

A classic synchronous generator will be power regulated, giving it abilities to deal with local power imbalances. A wind turbine on the other hand, has an uncontrolled power input. The net inertial energy supplied by the wind turbine during a frequency response must be zero, by the premise of returning to nominal speed. In other words, inertial energy supplied to the grid must return. This responsibility falls to the only power regulators in the system, the primary regulation of the residual grid. Being already weakly regulated, the added responsibility of stabilising more rotating mass will cause longer sustained oscillations. A control design improving damping should therefore be considered and designed.

4.2.1 Auxiliary HVDC-Link Voltage Control

Simplicity is emphasised when designing the controller coupling the grid frequency to HVDC-voltage. By Scaled Deviation Mirroring (SDM, proposed in this thesis) of the onshore frequency on to the HVDC-voltage reference, the voltage regulator allow the voltage to swing with the onshore frequency (with a regulation delay). By SDM, a per unit deviation from nominal grid frequency yields a scaled deviation from nominal DC-voltage. The scaling (control gain, K_v) ensures that the voltage variations is within component limits, as power electronics is sensitive too high voltages. An advantage gained by mirroring the frequency response on to the DC-voltage, is that the capacitive storage contribute to thepower imbalance. A filter is added

to take care of minor disturbances. The block diagram is found in figure 4.4.

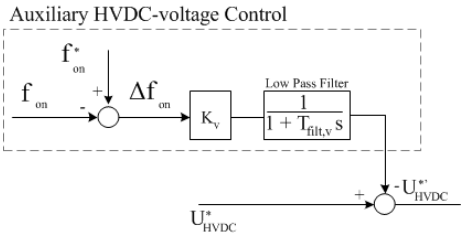

Figure 4.4: Block diagram of auxiliary HVDC-voltage control.

4.2.2 Auxiliary Offshore Frequency Control

The offshore frequency has the same auxiliary control as HVDC-voltage, SDM. The input is then DC-voltage, which deviation in per unit is mirrored and scaled to regulate the offshore frequency. The scaling, K_f, is inverse to K_V, such that the offshore frequency deviation is given the same amplitude as the onshore frequency. A filter is added as well. The resulting block diagram is found in figure 4.5.

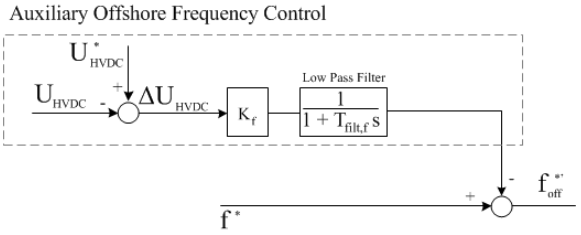

Figure 4.5: Auxiliary offshore grid frequency control by DC-voltage measurement

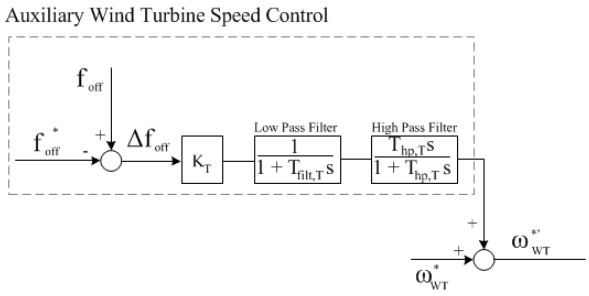

Figure 4.6: Block diagram of auxiliary wind turbine speed controller by SDM.

4.2.3 Auxiliary Wind Turbine Speed Control

The VSC-control has one inner- and one outer control loop (speed- and torque-control), and both references can be modified. The work presented in [16] use inner loop reference (torque reference) to produce an inertial response. It can be argued that the skipping the outer control loop would increase responsiveness of the auxiliary control, and consequently deliver inertia reserves more quickly. However, the design chosen in this thesis use the outer loop reference (speed reference). In fact, the full control strategy include a purposely delayed wind turbine inertia response to improve the system frequency response. The full reasoning to this design is made in the upcoming sections. This does however mean that the speed controller does not need to be very responsive (within reasonable limits).

Scaled Mirrored Deviation Control

This method is based on the same chain of thoughts as for the auxiliary HVDC-voltage control and offshore frequency control. By the offshore frequency measurements, the speed reference is modified by a term from an auxiliary turbine speed controller. The frequency deviation in per unit is simply multiplied with a gain and added to the speed reference. As listed in criteria for operation, the speed must return to its nominal speed in order to produce nominal power. This is done by a high pass filter with a high time constant, which removes steady state deviations without restricting the responsiveness. A low pass filter is also added to remove noise from measurements. The resulting control is then given by figure 4.6. Neglecting speed regulation delays, the auxiliary HVDC-voltage and offshore frequency control allows the wind turbine inertia response to be in phase with frequency response.

Wind Turbine Stabiliser Control

Frequency mirroring will in theory make the wind turbine swing as synchronous generators, though with an inevitable delay due to limited regulation quickness. It was predicted that oscillations would be longer sustained by the demand for power in bringing the wind turbine back to nominal speed. To deal with such behaviour, a controller contributing to damping should be designed. The input should still be offshore frequency, and the wind turbine rotational speed is the control objective.

To contextualise the WTS-control, the Power System Stabiliser is presented. The PSS is an effective way of providing damping. Classical PSSs can use various parameters as input and by a control structure producing a phase leading term, either voltage- or governor reference is modified (E-PSS and G-PSS, presented in article [17]). The result is a phase leading power production, contributing to damping. Details on PSS implementations can be found in [8], ch. 10.1. An extensive evaluation of PSS tuning techniques is presented in [18]. This paper aims to highlight the qualitative effect of such systems, and optimal tuning is therefore not emphasised.

Consider a very simple power system with one bus, two governor controlled synchronous generators (0.5 *p.u.* each) and a load (1 *p.u.*), figure 4.7. The power balance is maintained by the coordinated governor actions of the two generators. It is assumed that the performance of generator B can not be changed or improved, i.e. connected by a high impedance (weak grid characteristics). Imposing a load disturbance will invoke a primary frequency response as discussed in chapter 2. The initial frequency drop is determined by the magnitude of the power disturbance and system inertia. The stabilisation of the system is determined by the regulatory performance of the governors.

Assume one want to enhance the damping of the system by implementing a PSS to the governor of generator A. By the technique presented in chapter 10.1.2 in [8], the governor is controlled so that the mechanical power is phase leading the rotational speed, providing damping.

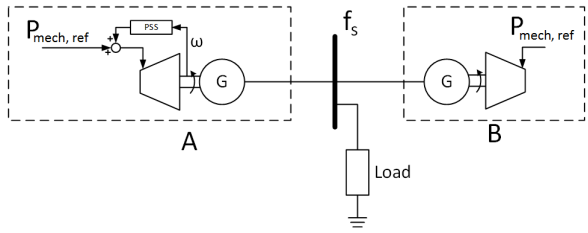

Figure 4.7: Simple power system with implemented Governor-PSS.

Then, the generator A is replaced by full converter wind turbines, represented by a single turbine, figure 4.8. The behaviour of this generator differs in two distinct ways. Firstly, the generator side frequency is operated independently from the synchronous system, meaning full speed control of the generator. Secondly, there are no governor action, meaning any imbalance between mechanical and electrical power, must be supplied or received by the residual grid. It is assumed that the FCWT has been implemented with auxiliary speed control such that it swings perfectly with the grid frequency, as a synchronous generator. Regulation delays are neglected.

The differences in generator behaviour (with SDM-control) fundamentally changes its interaction with the grid. During an initial frequency drop, the wind turbine provides inertial energy as a classic synchronous generator. But when frequency drops, the classic synchronous generator would have governor control, *providing* power to accelerate back to nominal speed. A wind turbine on the other hand, *demands* power from the grid when accelerating. Assuming an inertia constant of wind turbines to be about twice that of a classic generators, the governor in B must suddenly accelerate and stabilise 3 times the rotating mass as before. The result is longer sustained oscillations, though smaller in magnitude.

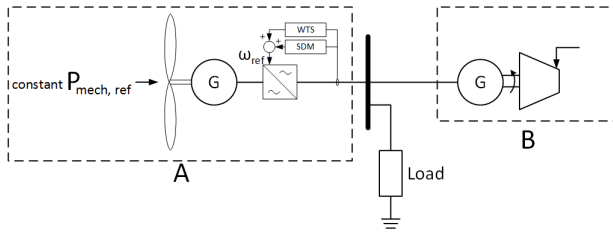

Figure 4.8: Simple power system with 50% wind power share.

When designing the wind turbine stabiliser, the idea is funded on the principle of PSS - a phase leading term providing damping power. No changes can be made to the control of generator B. The point of the previous discussions was to illustrate that the system is less stable due to the wind turbines dependency on grid governors. But this is also the key to designing the WTS. Since the wind turbine demands power, rather than providing power following a inertia response, the tuning of the stabilise control should also be opposite. As the wind turbines are a major source of oscillations, the grid power should be phase leading the wind turbine frequency in order to damp oscillations. This can easily be realised by the flexibility of local frequency control. In other words, by a controlled phase *lag* in the wind turbine frequency response, the grid side will act as if PSS-controlled.

The idea is simple, but there are a few points that should be discussed.

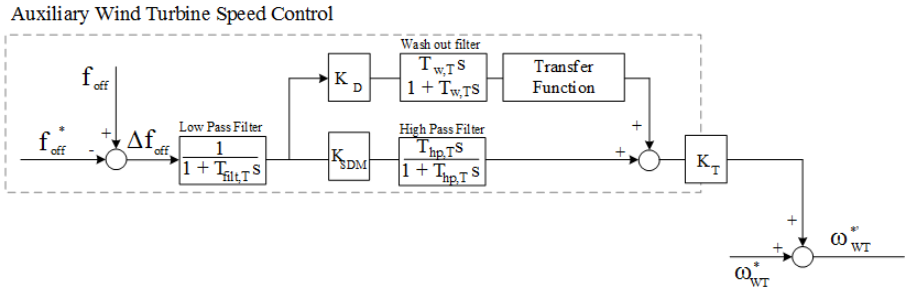

Figure 4.9: Block diagram of auxiliary wind turbine speed controller by SDM and WTS.

Assuming that the speed response nadir of the wind turbines is equal with and without WTS implemented, the onshore frequency response nadir would be lower, due to the delayed contribution from the wind turbines. Also, the effectiveness of the damping would strongly depend on the total wind power share in the system.

The WTS-control structure is more or less equal to a PSS, and is given by equation 4.1. The complete design for auxiliary turbine speed control is given as a block diagram in figure 4.9. The key difference is the tuning of parameters in order to make the phase contribution negative. This is demonstrated at a later stage.

$$x = K_D \frac{sT_w}{1 + sT_w} H_D(s)\, y \tag{4.1}$$

Chapter 5

Method

5.1 Simulation model

A simulation model is beneficial in order to make some predictions in preparation of laboratory work. This is done by expanding the model developed in a previous thesis [16]. Note that the model is rebuilt from scratch and differences may occur. The simulation model is summarised in appendix D. MatLab SIMULINK is considered the best tool for such a simulation. As the model is chosen to be mathematical, rather than electrical, the basic SIMULINK library with continuous calculations can be utilized. This is desirable in order to model physical systems and controllers flexibly. The fact that previous work with such a model found good correlation between laboratory and simulation results is also contributing to the choice of this simulation tool.

5.1.1 Model Overview

There are some main simplifications that should be covered prior to presenting the model. The model work in per unit values, eliminating AC/DC-considerations. Losses are neglected. The weak grid is modelled in order to mimic a behaviour we recognise as characterising for a weak grid. This implies poor ability to stabilise the system, both by its closeness to disturbances (high connective impedance) and its total inertia. In section 2.1.1 we found that a low system inertia leads to high deceleration. The power should be speed-droop controlled. A PI controller is used, in anti-parallel with the droop gain, ρ, according to equation 2.2. Rotor angle swings are neglected. The system equation is described by the swing equation, 2.1. The resulting block diagram,

All derivation of block diagrams for converter control and system equations were made in section 3. These are directly implemented in the simulation model. The simplifications for these controls were justified in the corresponding sections, and we assume them equally valid in simulation work.

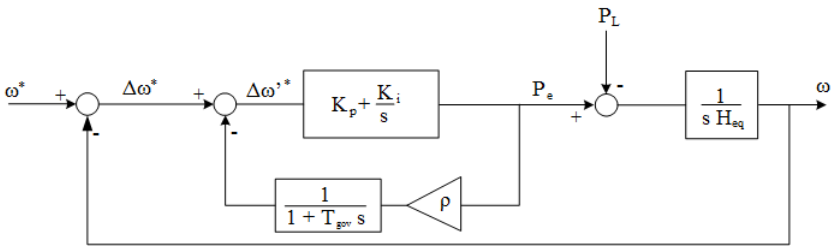

Figure 5.1: Block diagram of weak grid model

The auxiliary control is also directly given by the processes given in section 4.2. The simulation model found in appendix D.

5.2 Laboratory

The laboratory is provided by SINTEF Energy Research and NTNU. Data of laboratory components are covered by the data sheets provided by NTNU and Sintef [20, 21, 22, 23, 24, 25].

5.3 Equipment

The laboratory is equipped with the following components which are utilized. The relevant setup is given by figure 5.2.

- Weak Grid equivalent - induction motor-synchronous generator set with variable speed drive
- Controllable load
- 2 Voltage Source Converters
- Frequency converter (Back-to-back VSC)
- DC-cable equivalent
- Converter control by LabView

5.3.1 LabView

LabView is a graphical programming environment, enabling communication with physical components, including control and measurements [20]. The program is custom made in order to realise the system of investigation. The

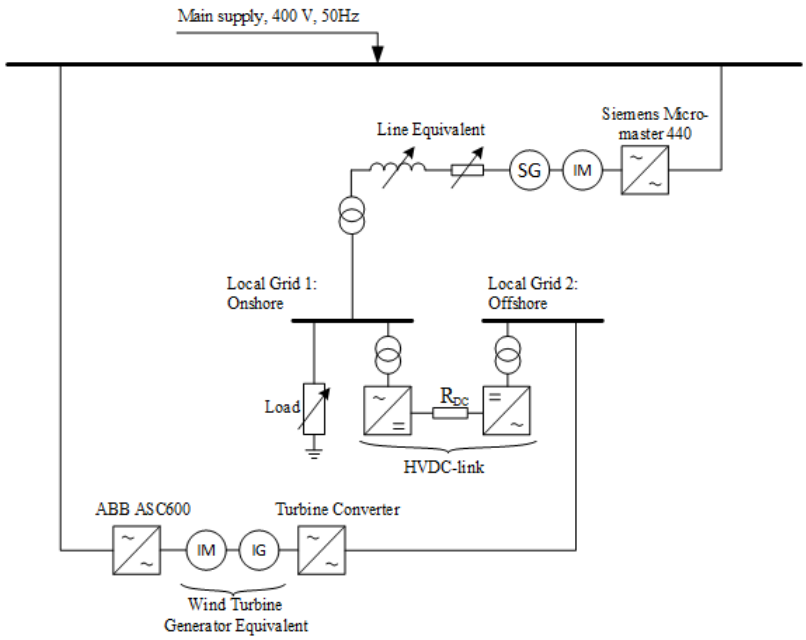

Figure 5.2: Laboratory setup

program is equal to that used in [16], but new support strategies are implemented.

5.3.2 Grid Equivalent

The weak grid equivalent consists of a synchronous generator powered by a induction motor drive connected through a variable transmission line equivalent and a transformer. The drive for the induction motor is rated at 22kVA. It is vector controlled with a speed encoder and droop control to emulate a classical power system. The motor and generator specifications are found in table 5.1 and 5.2 respectively. The per unit base for inertia constant calculations is 17 kVA

A 22 kW frequency converter is used to drive the induction motor. A speed encoder uses measurements in order to vector control the motor, mimicking droop control and governor settings of a power plant. A variable transmission line is connected to the grid equivalent. A 400:400 V transformer is placed in connection to point of common coupling, defined as the joint busbar of the grid, load and converter.

Table 5.1: specifications of laboratory synchronous generator in grid equivalent

Parameter	**Value**
Rated power, S_n	17 kVA
Rated voltage, V_n	400 V
Rated power factor, $cos(\phi)$	0.8
Rated speed, ω_n	1500 rpm
Inertia constant,H_{eq}	0.84 s (17 kVA base)

Table 5.2: specifications of laboratory induction motor in grid equivalent

Parameter	**Value**
Rated power, S_n	18.5 kVA
Rated voltage, V_n	380-414 V
Rated power factor, $cos(\phi)$	0.86
Rated speed, ω_n	1465 rpm

5.3.3 Voltage Source Converters

The VSCs are developed and built by SINTEF Energy Research. They are designed highly flexible, and all control parameters are available through a FPGA-based processor system.

Table 5.3: specifications of laboratory Voltage Source Converters

Paramenter	**Value**
Rated power, S_n	60 kVA
Supply voltage, V_{ac}	380-414 V
Rated current, I_{ac}	100 A
Maximum switching frequency, f_s	7000 Hz
LCL-filter	500 μH, 50 μF, 200 μH
DC-filter capacitance	14 mF

5.3.4 Wind Generator Equivalent

The wind turbine equivalent is a induction motor-generator set, details given in table 5.4. It can be driven by a frequency converter from ABB (ABB ACS600), which is a 400 V AC, 75 kW converter. As the system is very simple, the power flow is less important, and the wind turbine equivalent is therefor run as a motor rather than a generator. This ensures that the frequency converter, ACS600, doesn't influence the results by its inherent dynamic behaviour. Since the inertial behaviour is the system is to be investigated, the origin and total amout of power is irrelevant.

Table 5.4: specifications of laboratory wind turbine equivalent

Parameter	**Value**
Rated power, S_n	55 kVA
Rated voltage, V_n	380 V
Rated power factor, $cos(\phi)$	0.81
Rated speed, ω_n	990 rpm
Inertia constant,H_{eq}	3 s (NB! 17 kVA base)

Chapter 6

Results

The control strategies is presented with the simulation model and laboratory setup as foundation. Simplifications presented in chapter 5 will be further supported by comparing initial test results. The laboratory model is incrementally expanded, and compared to simulation results. A validated simulation model is highly beneficial, as control design tools in MatLab can be utilised. A linearised model is made in Matlab, and its relevant Bode- and Pole-Zero-plots is presented.

A reference system set up is chosen while initiating laboratory testing. This includes determining settings for governor, load size, wind power share, nominal speeds and –voltages. By choosing a proper reference system, the expansion of the system can be done in a controlled manner. It is also important to establish good results to which further results can be compared. The simulation- and laboratory model are compared and validated in appendix C. The desired characteristics of the reference case should be;

- The frequency stability of the grid should be poor, that is high frequency deviation and sustained oscillations.
- The wind turbine should have a adequately quick speed control to facilitate optimize power production.
- The VSC-control should be quick and tuned for good performance.
- The distribution of inertia reserves should reflect a realistic power system.

The wind turbine equivalent is run at $500rpm$, which is half of nominal speed from which the inertia constant is calculated. Referring to section 2.1.1, half nominal speed equals a quarter inertia constant. Then the inertia coefficient is then 0.75 s (referred to table 5.4). The equivalent inertia coefficient of the grid is 0.84 s. It is calculated in [19] that a wind turbine of the current size has a inertia constant of about, $9-10$ s related to local nominal power. A grid would have an inertia of about $2-10$ s depending on stiffness/weakness. It is recognised that the inertia of the laboratory is quite low, but since this is a qualitative assessment of frequency response, this is less important. The critical measure is the distribution of the inertia, and it is close to 50-50 between the grid and the wind farm equivalent in the lab. Assuming a real

Table 6.1: Parameters for frequency mirroring over HVDC-link

Parameter	**Value**
K_V	0.5
$T_{V,filt}$	0.01 s
K_f	2
$T_{f,filt}$	0.01 s

world system with an equivalent grid inertia constant of 4.5 s and the wind farm equivalent time constant of 9 s, a close to 50-50 distribution of inertial energy would yield a 33 % wind power share.

The governor settings are set to weak grid behaviour. The details are found in appendix C. The frequency response of the system with no auxiliary controls is given in figure 6.1. The responses match remarkably well.

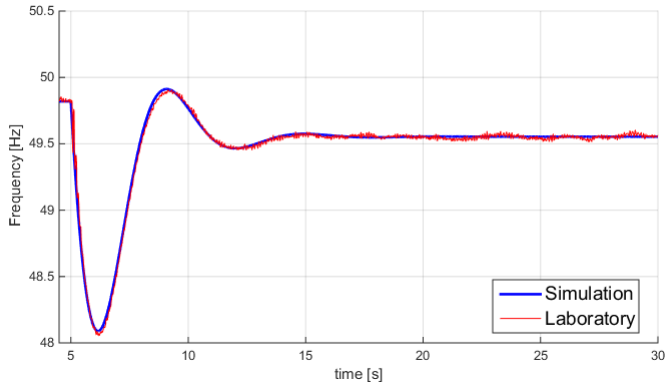

Figure 6.1: Frequency response imposing a load step of 0.0588 p.u.. Results from simulations and laboratory

6.1 Auxiliary HVDC-control

The HVDC-control strategy has been presented in chapter 4. The basic idea is to mirror the onshore frequency deviation to the offshore frequency. The method was abbreviated SDM, Scaled Deviation Mirroring. Figure 4.4 and 4.5 shows the block diagram of the proposed controllers. The parameters of said controller is given by table 6.1.

To confirm HVDC-regulation performance, the controllers are tested incrementally. The HVDC-voltage is initially regulated by imposing a fictitious

onshore frequency disturbance by a step. The lab set up is given by figure 6.2. The fictitious frequency step is made by subtracting 1 Hz from the onshore frequency measurement used in auxiliary HVDC-voltage regulation. In operation, any power system with rotating mass would be unable to make a frequency step, but follow a response similar to figure 6.1. This test is made in order to investigate the performance of the HVDC-voltage- and frequency regulation. Figure 6.3 shows how the offshore frequency follows the onshore frequency in simulations and laboratory. Figure 6.4 shows the bode plot of offshore frequency with onshore frequency as control variable by MatLab linerisation. Effective regulation is observed for frequencies below 1 Hz. Once again visiting figure 6.1, the oscillation frequency is found to be $1,023\ rad/s$, which is within the effective regulated frequency band of the HVDC-control. To confirm this statement, the next test should be to mirror the frequency from onshore to offshore following a load step.

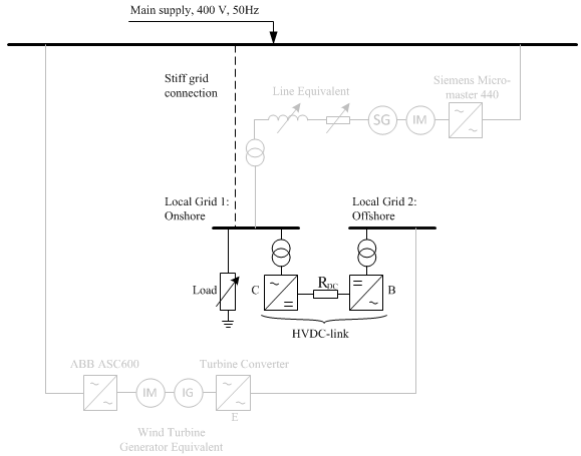

Figure 6.2: Laboratory setup for testing frequency mirroring from fictitious onshore frequency step.

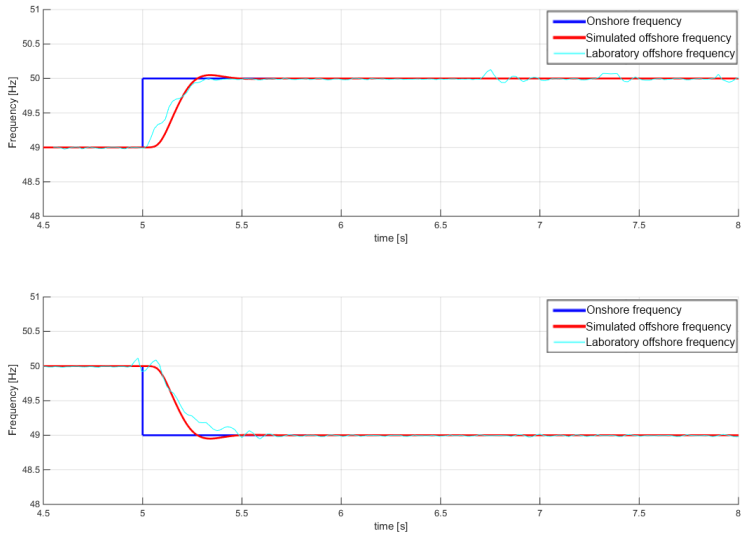

Figure 6.3: Offshore frequency response following a onshore fictitious frequency step.

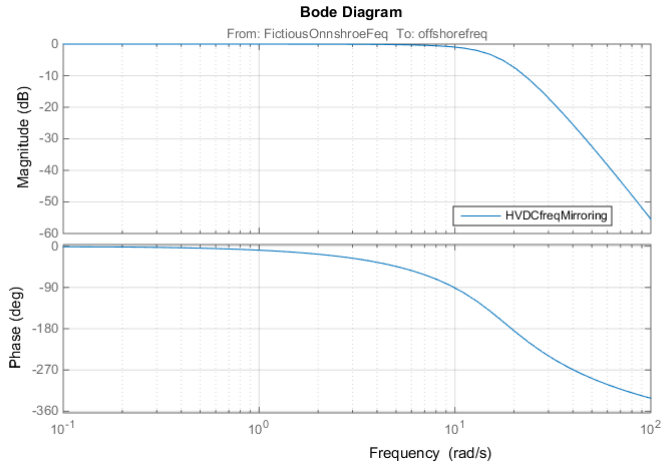

Figure 6.4: Bode plot of offshore frequency with onshore frequency as control variable with SDM-control in HVDC-converters.

The weak grid is connected to test frequency response with mirroring to offshore grid. Figure 6.5 shows the set up. At this point, some problems appeared in the lab. A resonance or measurement error created a high frequency noise or oscillating mode. Figure 6.6 shows how the onshore frequency during a time period with no perturbations to the system. The top plot shows disturbances seemingly appearing at random. The bottom graph is a 1.2 second part where the measurements show an obvious sine-wave oscillation indicating a resonance. This was further investigated at a later time, and measures taken to handle the resonance. This is presented in 6.3. For time being, the resonance is ignored.

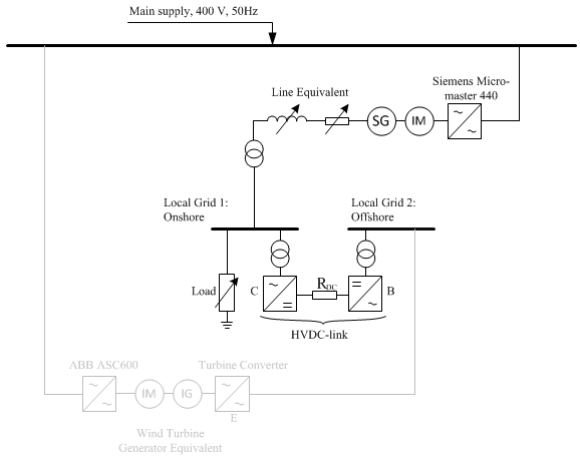

Figure 6.5: Laboratory setup for testing frequency mirroring from load disturbance.

When a load step disturbance is imposed, the onshore frequency follows the trajectory expected from earlier testing. Figure 6.7 shows that the frequency deviation is mirrored on to the offshore grid, and that there are good correlation between laboratory and simulated results. It is observed that there are a very short delay, which is promising for further testing. It should be noted that the resolution of the offshore frequency reference is high, 0.1 Hz. This creates a stair response. Until other results prove different, this effect is deemed non influential.

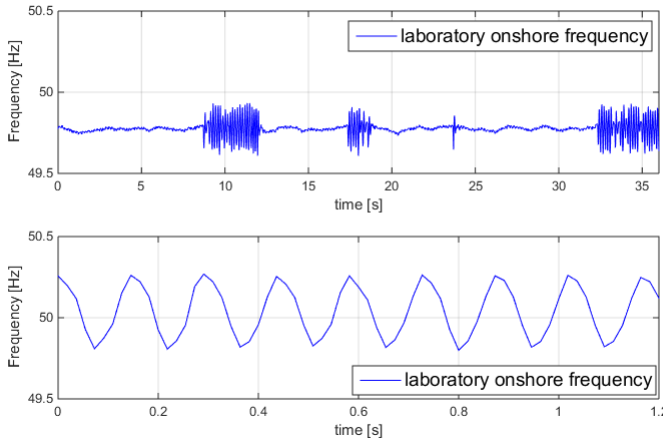

Figure 6.6: Laboratory measurements of onshore frequency showing a reappearing resonance. Over: reappearing resonance over longer time span, under: section of the resonance

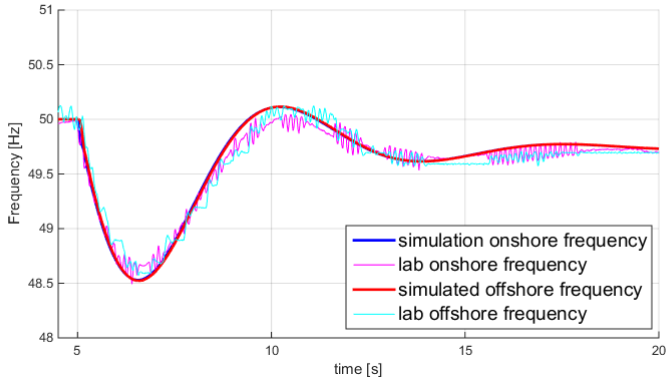

Figure 6.7: Mirrored frequency over HVDC-link.

6.2 Auxiliary Turbine Speed Control

6.2.1 Grid Connected Turbine

Initial testing of the turbine control system is made without including the HVDC-link. Figure 6.8 shows how the HVDC-link is short circuited by direct connection between Local Grid 1 and 2. The settings for the auxiliary control is given by table 6.2.

Table 6.2: Auxiliary FCWT-control parameters.

Parameter	**Value**
$T_{T,filt}$	0.01 s
K_{SDM}	1
$T_{hp,T}$	10 s
K_D	2
$T_{w,T}$	10 s
Transfer function	$\frac{1}{1+3s}$

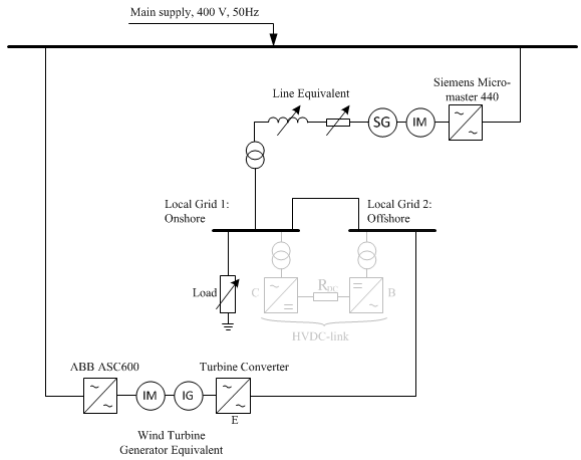

Figure 6.8: Laboratory setup for initial testing of inertia support from the wind turbine excluding the DC-link.

Scaled Deviation Mirroring Control

The auxiliary wind turbine control is done equally in laboratory and simulation model. The block diagram is given in figure 6.9. At first hand, the Wind Turbine Stabiliser Control is not implemented.

The frequency response of the onshore grid when imposing a load step, is found in figure 6.10. The response matches well, but there are deviations in first half period of the $\sim 10\ s$ oscillation. The Rate of Change of Frequency (ROCOF) during the first 3 *sec* seem to match the results with no auxiliary controls implemented. This may be due to a delay in the regulation, an oscillatory mode invoked be electrical transients, or voltage regulation. It is observed that the deviation from the simulation model is gone after some seconds. A discussion to the origin of this deviation is made in 7.5.

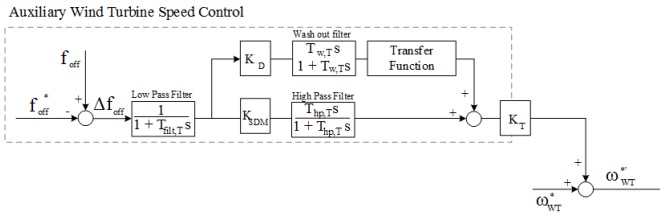

Figure 6.9: Block diagram of wind turbine speed and auxiliary turbine speed control.

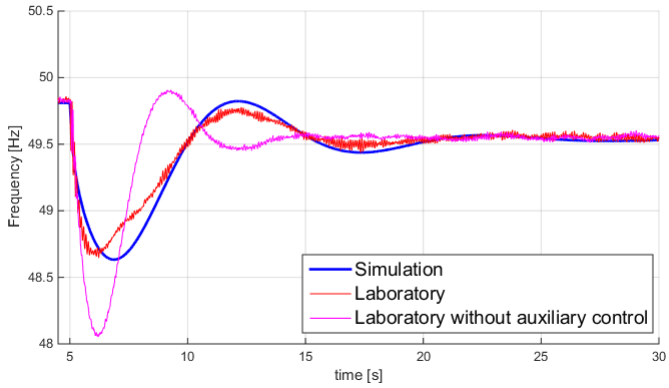

Figure 6.10: Frequency response of onshore grid imposing a 0.0588 p.u. load step in laboratory and simulation with implemented SDM-control in grid connected wind turbine.

Adding Wind Turbine Stabiliser Control

Section 4.2.3 proposed a design for better performance. The theory is that a phase lag in the frequency response of the wind turbine will improve damping. Since governors of conventional generators are responsible for stabilising the system, it only make sense that the onshore frequency should be leading the wind turbine frequency. This is based on the theory that a phase leading term provides damping and that the grid governors is responsible for damping the entire system. Equation 6.1 is the transfer function of the WTS-control,

$$Tf_{WTS}(s) = K_{WTS} \frac{T_{WTS}s}{1 + T_{WTS}s} \frac{1}{1 + T_{comp}s} \tag{6.1}$$

Figure 6.11 shows the onshore frequency response imposing the same load step response as before. The correlation between laboratory and simulations are adequate, but similarly as for testing with SDM-control only, there are an additional mode with unknown origin.

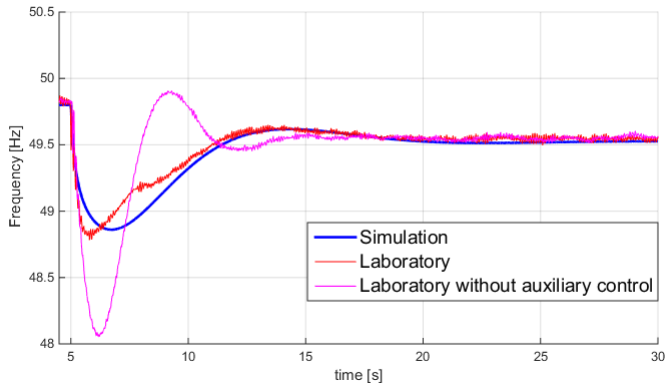

Figure 6.11: Frequency response of onshore grid imposing a 0.0588 p.u. load step in laboratory and simulation with implemented SDM- and WTS-control in FCWT connected to grid.

Bode-evaluation

Though an oscillation with unknown origin is present, a linearisation of the system is still valid in evaluating the dominant oscillation. By using control analysis tools in MatLab, a linearised model can be made and the oscillating behaviour quantified. The control variable is load power.

Table 6.3: Dominant poles observed as oscillations in frequency response plots with load as control variable with grid connected turbine (HVDC-link excluded).

Auxiliary Control	**Complex Pole**	**Natural Frequency,** ω_0	**Damping,** ζ	**Damped Frequency,** $\omega_d = \omega_0\sqrt{1-\zeta^2}$	**Oscillation Period** $t = \frac{2\pi}{\omega_d}$
No	$-0.481 \pm j1.07$	1.18 rad/s	0.408	0.97 rad/s	6.47 s
SDM	$-0.210 \pm j0.6$	0.635 rad/s	0.33	0.566 rad/s	11.1 s
SDM and WTS	$-0.269 \pm j0.432$	0.509 rad/s	0.53	0.431 rad/s	14.56 s

Three systems (without auxiliary control, with SDM, and with SDM and WTS) are linearised, and the poles are plotted in the same imaginary plane. They are 3, 14 and 16 state space models respectively. Figure 6.12 shows all poles, but since most poles with system impact (visible in the frequency response) are very close to the origin, a zoomed plot is more easily examined, figure 6.13. Information on the dominant poles is summarized in table 6.3.

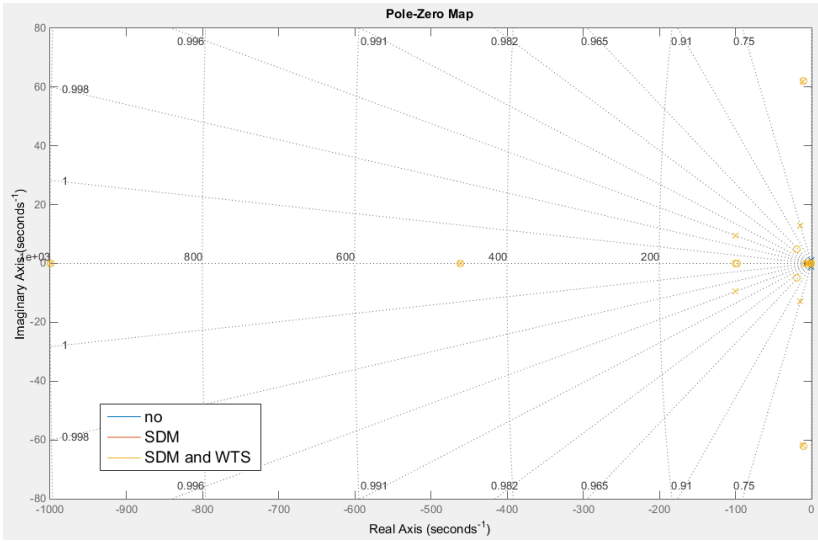

Figure 6.12: Pole-Zero-diagram of the linearized model with load power as control variable and onshore frequency as output state variable, with HVDC-link excluded.

The data from table 6.3 verify the linearisation to a great degree. The damped frequencies correlate with the response in figure 6.10 and 6.11, and the general impression from the damping fits with the relation between damp-

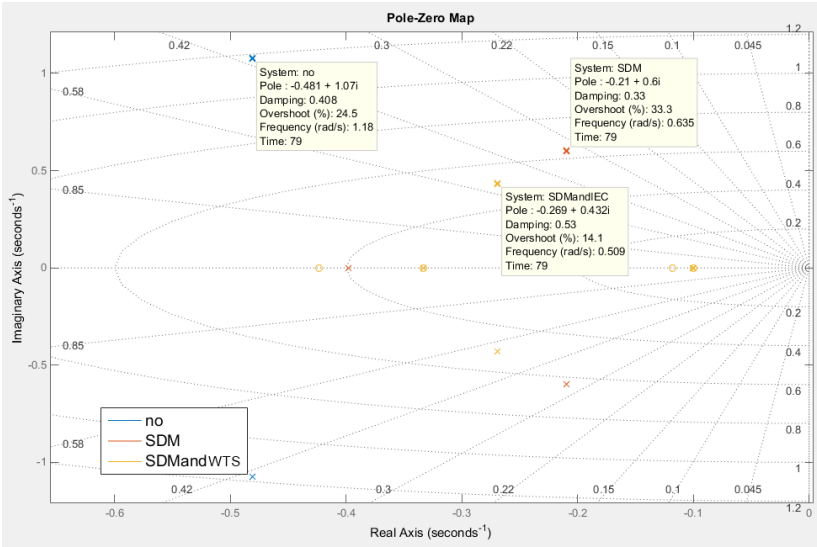

Figure 6.13: Zoomed Pole-Zero-diagram of the linearized model with load power as control variable and onshore frequency as output state variable, with HVDC-link excluded.

ing constants. The introduction of auxiliary SDM-control contributed in reducing the frequency drop, but introduced more oscillations. This was predicted, and confirmed by a lower damping constant ζ. By the prediction, the WTS-control was designed. Further reduction of frequency drop, in addition to a greatly improved damping is a testament to the effectiveness of the WTS-control.

The details of the WTS-control behaviour can be observed by the bode-plot 6.14. Section 4.2.3 proposed a wind turbine frequency response lagging the grid frequency response to improve damping. The phase lag is observed in the bode plot, and range from 6.47 $s \approx 1$ rad/s to 17.16 $s \approx 0.36$ rad/s. The damped frequencies from table 6.3 is within this range.

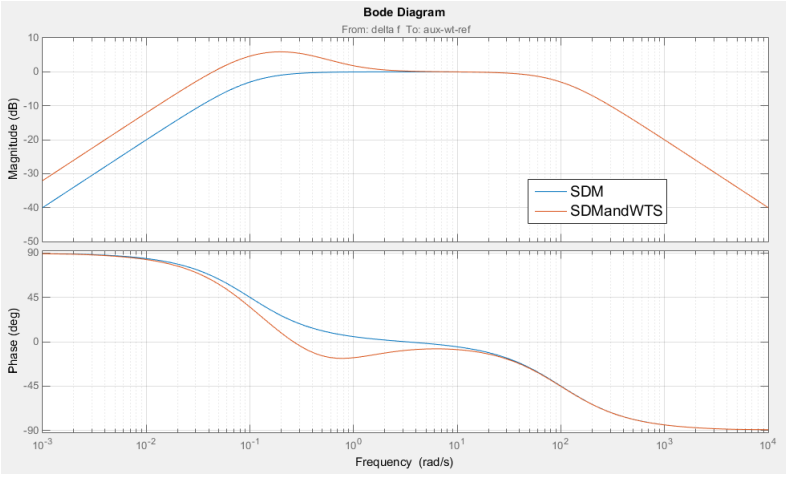

Figure 6.14: Bode plot of wind turbine response with offshore frequency deviation as control variable.

6.2.2 HVDC-connected Turbines

With auxiliary wind turbine control implemented and tested, the system can be expanded to its full configuration, including the HVDC-link. The lab configuration is given by figure 6.15. In section 6.1 the HVDC-control was tested, and revealed problems with noise or resonance, these are neglected until further notice. The auxiliary control parameters is given by table 6.4. The parameters is referred to figures 4.4, 4.5and 4.9.

Table 6.4: Auxiliary control parameters of full system configuration.

Parameter	**Value**
HVDC-voltage	
K_V	0.5
$T_{V,filt}$	0.01 s
Offshore Frequency	
K_f	2
$T_{f,filt}$	0.01 s
Wind Turbine	
$T_{T,filt}$	0.01 s
K_{SDM}	1
$T_{hp,T}$	10 s
K_D	1.5
$T_{w,T}$	10 s
K_T	1
Transfer function	$\frac{1}{1+3s}$

Scaled Deviation Mirroring Control

The same test is conducted as in section 6.2.1, by a 0.0588 $p.u.$ load step onshore. The onshore frequency response is given by figure 6.16. The correlation between laboratory and simulation is good, apart for the mode/delay mentioned before. This is further discussed in section 7.5. Figure 6.17 shows the speed response of the wind turbine gathered from simulation and laboratory.

Adding Wind Turbine Stabiliser Control

Including WTS-controllers improves the behaviour as expected, figure 6.18. Good correlation with simulation model is still found. It is observed that

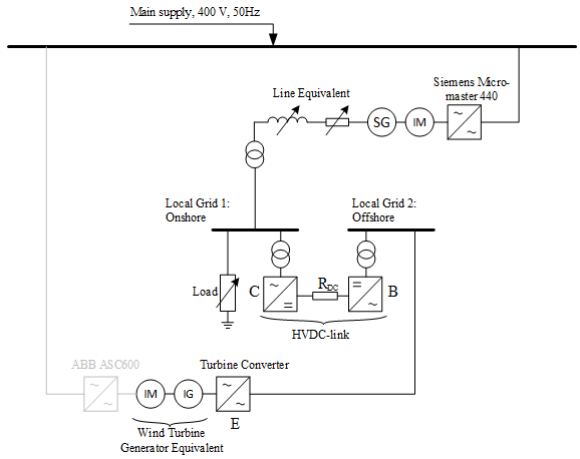

Figure 6.15: Laboratory setup of full system including full converter wind turbine and HVDC-link.

the quick regulation over the HVDC-link does in fact allow for the HVDC-connected turbines to provide inertia support about as efficiently as grid connected turbines. A more thorough evaluation of performance is made in chapter 7. Figure 6.19 shows the speed response of the wind turbine gathered from simulation and laboratory.

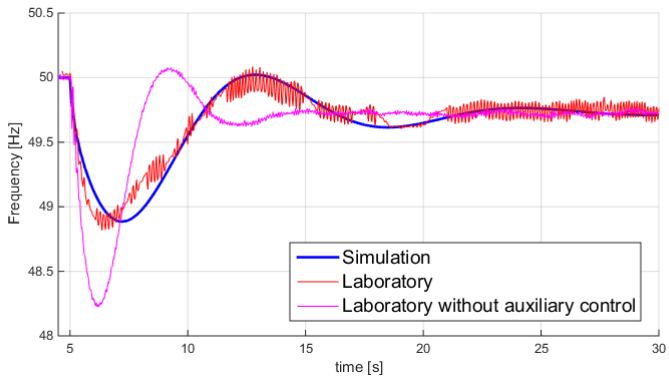

Figure 6.16: Frequency response of onshore grid imposing a 0.0588 p.u. load step in laboratory and simulation with implemented SDM-control in HVDC-connected FCWT.

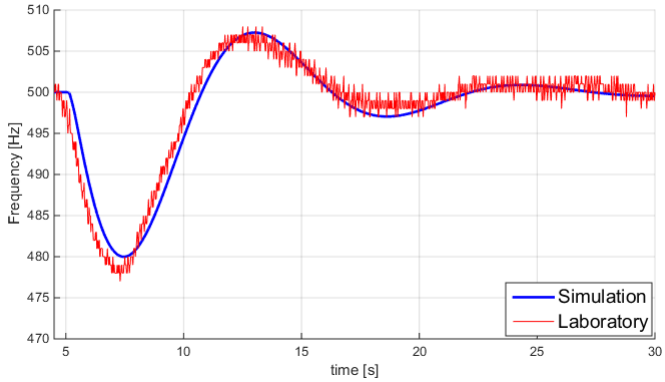

Figure 6.17: Wind turbine speed response when imposing a 0.0588 p.u. load step. Results from laboratory and simulation with implemented SDM-control in FCWT connected by HVDC to the grid.

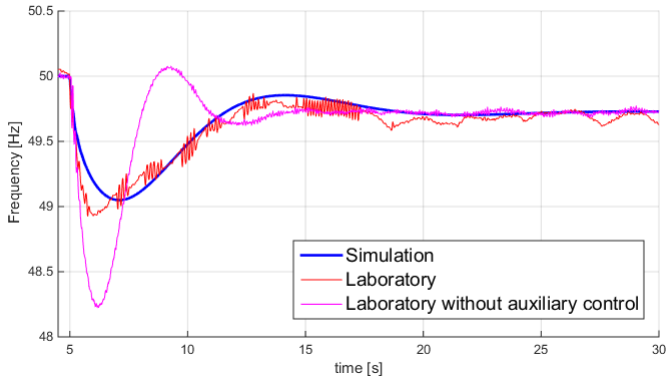

Figure 6.18: Frequency response of onshore grid imposing a 0.0588 p.u. load step in laboratory and simulation with implemented SDM- and WTS-control in HVDC-connected FCWT.

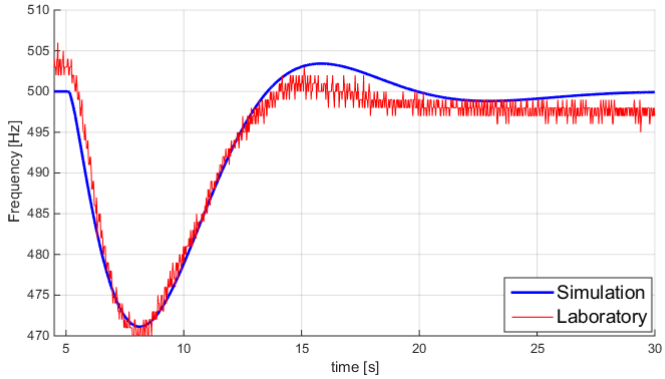

Figure 6.19: Wind turbine speed response when imposing a 0.0588 p.u. load step. Results from laboratory and simulation with implemented SDM- and WTS-control in FCWT connected by HVDC to grid.

Bode-evaluation

The same method for linear analysis as used in 6.2.1. Three systems (without auxiliary control, with SDM, and with SDM and WTS) are linearised, and the poles are plotted in the same imaginary plane, figure 6.20. Information on the dominant poles is summarized in table 6.5.

Table 6.5: Dominant poles observed as oscillations in frequency response plots with load as control variable in full system configuration.

Auxiliary Control	**Complex Pole**	**Natural Frequency,** ω_0	**Damping,** ζ	**Damped Frequency,** $\omega_d = \omega_0\sqrt{1-\zeta^2}$	**Oscillation Period** $t = \frac{2\pi}{\omega_d}$
No	$-0.481 \pm j1.07$	$1.18\ rad/s$	0.408	$0.97\ rad/s$	$6.47\ s$
SDM	$-0.177 \pm j0.559$	$0.586\ rad/s$	0.303	$0.558\ rad/s$	$11.25\ s$
SDM and WTS	$-0.234 \pm j0.424$	$0.484\ rad/s$	0.484	$0.348\ rad/s$	$14.83\ s$

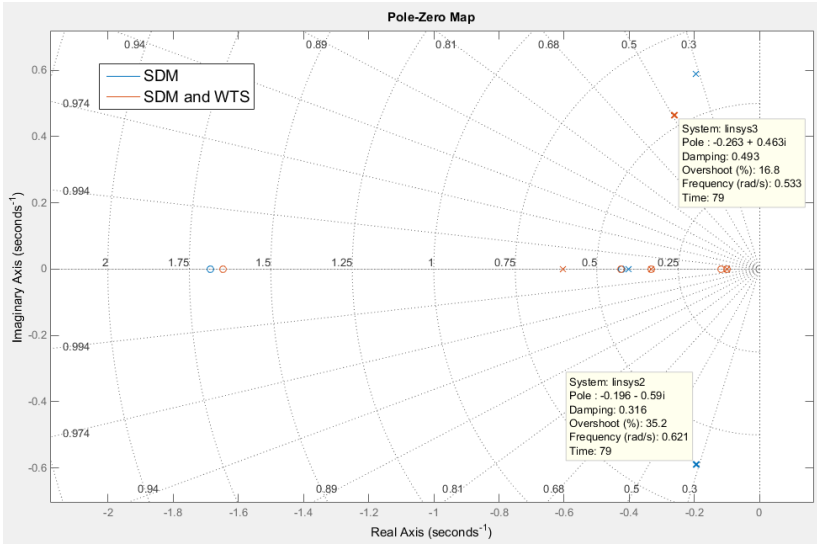

Figure 6.20: Zoomed Pole-Zero-diagram of the linearised model with load power as control variable and onshore frequency as output state variable, full system configuration.

6.3 Resonance

It was discovered that the auxiliary control invoked a resonance of some sort, and an investigation is made to clarify the origin. By investigating response from different perturbations to the laboratory setup, the resonance appear to be a result of multiple unfortunate characteristics. The following discussion does however propose a simple solution. The observations include;

- The sampling time of the control program, in LabView, is quite high. Experiments showed that the oscillation frequency was directly related to the sampling time, figure 6.21.
- There was a problem found with the PLL-control structure. This error was found on a very low level in the FPGA programming, and even in circuit board components. The effect of these errors is hard to predict, but a relation to the resonance can not be ruled out. The sudden jumps in DC-voltage would stress the PLL-controller.
- The DC-voltage and frequency seem to be oscillating in opposite phase, figure 6.22, though the voltage resolution makes the results hard to interpret. The sampling time has been tripled to induce higher oscillations. The power is plotted with onshore frequency in figure 6.23 and confirms the suspicion of opposite phase, considering that the power balance, $\Delta P = P_L - P_{grid} - P_{hvdc}$, must be 180° phase shifted due to the sign of P_{hvdc}, and by the knowledge that frequency is 90° phase lagging power, [8], ch. 5.5.3.
- The DC-voltage reference has quite high resolution, as viewed in figure 6.22. By the capacitive energy stored in the DC-link, voltage jumps give power surges. Figure 6.23 show power flow with the characteristics of a charging and discharging capacitance.

By combining these observations it can be argued that an unpredictable PLL-behaviour makes the frequency-DC-voltage coupling behave strangely, resulting in a highly varying DC-voltage. The high resolution DC-reference produce power surges. Since the oscillating frequency is high, its outside the bandwidth of the governor (see figure C.2). The frequency is then behaving as unregulated, lagging the power imbalance by 90° (the power imbalance will be 180° shifted compared to the Active power of converter C). It should be noted that the frequency of the resonance is close to that of the PLL-damped response, figure C.10.

An additional observation can be made by analysing the linearisation results of the simulation model. Figure 6.24 shows the bode plot with onshore frequency as control variable and DC-voltage as output, reveal that there are a unfortunately high gain for frequencies lagging close to 180° and more.

The onshore frequency oscillation periods from figure 6.23 are about 0.12 s, or about $53 = 10^{1.7}$ rad/s. By investigating the area highlighter by a circle, gain of -10 $dB \approx 0.31$ correlates well with the voltage oscillations from figure 6.22. Using a frequency oscillation amplitude of 0.15 $Hz = 0.004$ $p.u.$ and the gain of -10 dB gives voltage oscillations with amplitude 0.75 V, which is consistent with the observations. The phase lag is significantly higher in the simulation model, but due to the number of simplifications, it is fair to assume that the source of resonance is found.

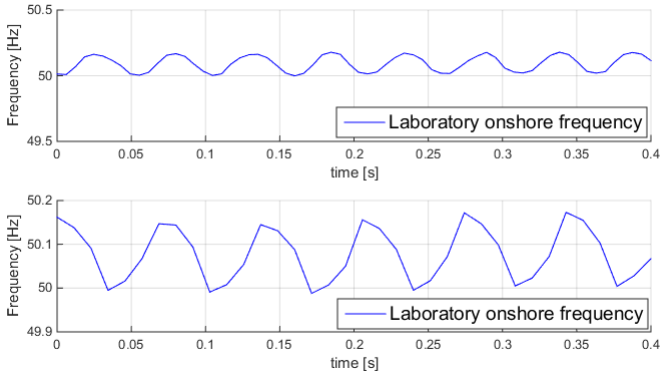

Figure 6.21: Section of resonance observed in laboratory when computing sampling time is low (12 ms) and high (30 ms).

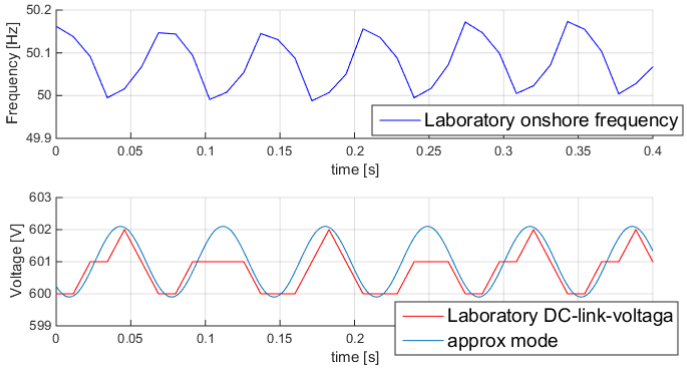

Figure 6.22: Section of resonance observed in laboratory when computing sampling time is high. An approximation of DC-voltage mode is included.

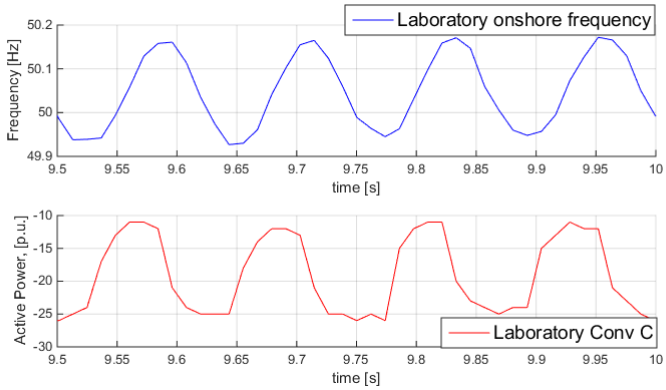

Figure 6.23: Section of resonance observed in laboratory showing power oscillations.

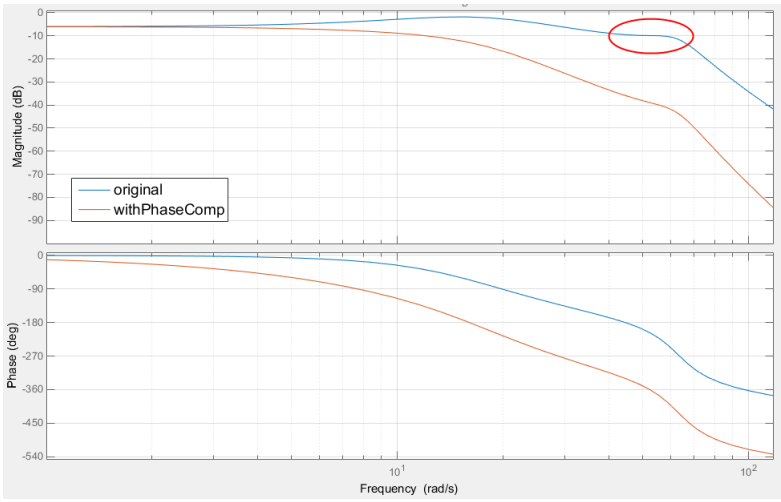

Figure 6.24: Bode-plot of the linearised model with onshore frequency as control variable and DC-voltage as output.

It is indicated in figure 6.24 that some measures could be taken to manage the resonance. A phase compensator is used to lower the gain in the relevant area. The phase compensator is given by equation 6.2, where y is input and x is output.

$$\frac{x}{y} = \left(\frac{1+T_1 s}{1+T_2 s}\right)^p = \left(\frac{1+0.001s}{1+0.1s}\right)^2 \tag{6.2}$$

The results of the implemented phase compensator is given in figure 6.25. It is the same test as in figure 6.7, but now without the resonance. There are some indications that the high resolution of the DC-voltage reference causes some problems still, without "triggering" an resonance.

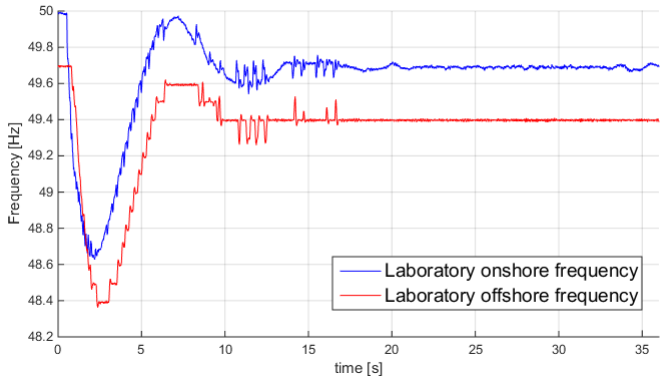

Figure 6.25: Bode-plot of the linearised model with onshore frequency as control variable and DC-voltage as output.

6.4 SDM- and WTS-control Interaction

In order to highlight the effects of the SDM- and WTS-controls in interaction with each other, an novice investigation of the tuning of the two are made.

A series of simulations is run with different gains (K_{SDM}, K_D and K_T). The goal of this test is to observe how the timing of the speed response alters the frequency response. The gain K_T is tuned in order for the speed drop to be of equal size. Then, by altering the relative contribution of K_{SDM} and K_D, the qualitative effects of the two control strategies should be visible by the both wind turbine speed response and onshore frequency response. The results are given by figure 6.26 and 6.27.

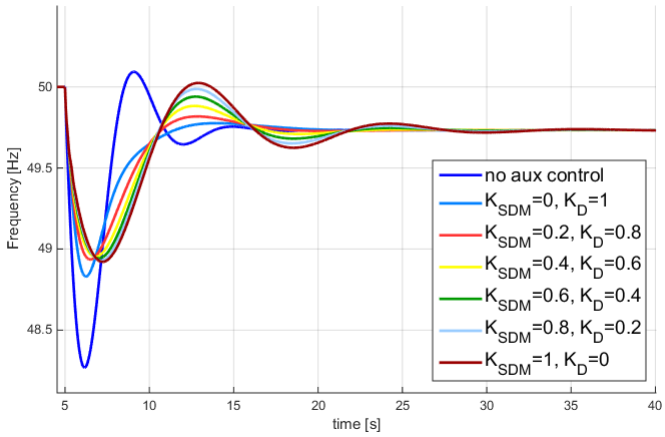

Figure 6.26: Frequency response of onshore grid from simulations when imposing a 0.0588 p.u. load step with HVDC-connected FCWTs and implemented SDM- and WTS-control with different K_{SDM}- and K_D-settings.

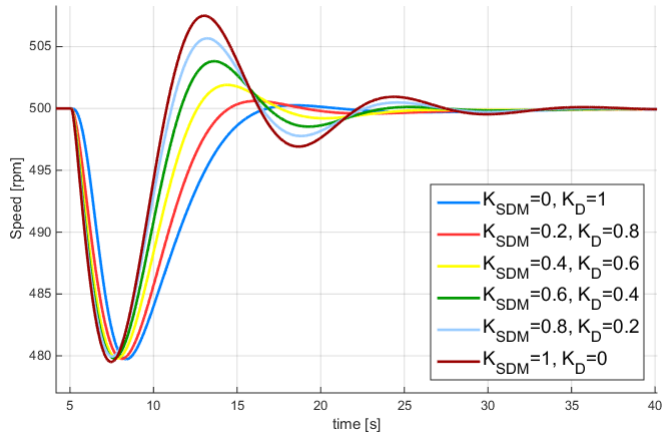

Figure 6.27: Wind turbine speed response from simulations when imposing a 0.0588 p.u. load step onshore, with HVDC-connected FCWTs and implemented SDM- and WTS-control with different K_{SDM}- and K_D-settings.

Chapter 7

Discussion

7.1 Performance

The sole purpose of designing auxiliary controllers for the HVDC-connected FCWT-farm was to improve the frequency dynamics of the system. The measures of improvement is frequency nadir and damping of frequency response.

Section 6.2.2 presented pole-zero plots demonstrating how the poles, and hence the oscillatory modes, was shifted by the introduction of auxiliary control. The inertia constant of the wind turbines is about 3.5 times higher than the grid equivalent inertia at nominal speeds, but as the wind turbines is run on half the rated speed, the wind turbines inertial energy is about 0.875 times that of the grid ($E_{rotational} = \frac{1}{2} I_{eq} \omega^2$). This would equal about 33 % wind power share, by the arguments given in the introduction of chapter 6.

Table 7.1: Frequency response performance for the HVDC-connected FCWTs with auxiliary controllers.

Auxiliary Turbine Controllers	Δf **[Hz/%]**	Δf**-reduction [%]**	$\Delta\omega_{WT}$ **[rpm]**	**Overshoot [Hz]**	**Overshoot reduction [%]**	**Sustained Oscillations [s]**
No	1.7 Hz	-	-	0.4 Hz	-	10 s
SDM	1.1 Hz	35.3 %	20 rpm	0.35 Hz	12.5 %	20 s
SDM and WTS, $K_T = 1$	1 Hz	41.2 %	30 rpm	0.15 Hz	62.5 %	15 s
SDM and WTS, $K_T = 0.66$	1.2 Hz	29.4 %	20 rpm	0.15 Hz	62.5 %	15 s

Revisiting the results from section 6.2.2, figure 6.16, 6.17, 6.18 and 6.19, the performance can be summarised by table 7.1. The calculations is made from laboratory results. The improvement is quite prominent, greatly reducing frequency drop and overshoot. The oscillations are longer sustained as the grid governors is given the responsibility of damping an increased rotating mass, though they are more efficiently damped when WTS-control is implemented. Details on WTS-control is given in the upcoming section 7.2.

It should noted that the speed response is greater in magnitude when WTS is implemented. New experiments are made to account for this difference. The gain K_T, figure 4.9, is adjusted so that the speed response is $20rpm$ with WTS-control. The results are found in appendix A, section A.1, and included in the summary in table 7.1. The performance is then worsened due to the delayed speed response (phase lag), but the damping effect is still prominent. Section 7.4 discus the limits of the speed response.

7.2 Wind Turbine Stabiliser Control

The WTS-control is a central part of the testing conducted in this thesis. The motivation of such a controller is the longer sustained oscillating behaviour invoked by the wind turbines interaction with the grid from an inertial response. With no governor control, the wind turbines provide inertial energy, but not contribute in regulating the system back to steady state. This can be compared to adding more inertia to the existing synchronous generators. With no improvement to the governors, they would have a harder time to stabilising the larger rotating mass.

The key in designing the controller is the completely decoupled frequency on the generator side of the FCWT. This flexibility is highly beneficial since the key in damping oscillations is contribution of power at the right time. The basic principle known from GPSSs (Governor Power System Stabilisers) is used - primary regulation phase leading rotational speed oscillations. By recognising that the wind turbines are stabilised by the primary regulation of the residual grid, the governor action should be phase leading the wind turbine inertia response, or equivalently, a wind turbine inertia response lagging the governor action. Since a lagged response means delayed contribution of inertial energy, the performance would be compromised. The performance will be a trade off between nadir and oscillations, determined by the gain of SDM- and WTS-control respectively.

The results from section 6.2.1 and 6.2.2 prove the design effective. The bode plot in 6.14 show that the auxiliary control produce a phase lag for frequencies from $0.031\ Hz \Rightarrow 30\ s/period$ to $0.31\ Hz \Rightarrow 3\ s/period$. Most frequency responses would be within this range.

How the gains K_{SDM} and K_D influence the behaviour was tested by simulations. The results are included in section 6.4. The immediate observation is that a very short delay in wind turbine response, greatly alters the frequency response of the system as a whole. The nadir of wind turbine speed is delayed by only a second-second and a half, but the effect is very prominent. In fact, it could be argued that in this specific configuration, using the WTS-control alone would be the optimal tuning.

It has been casually assumed that a quick wind turbine inertia response would reduce the initial ROCOF, and hence reduce nadir. The results in section 6.4 does however portrait another characteristic. From figure 6.27 it can safely be said that the speed response is quickest when excluding the WTS-controller all together ($K_{SDM} = 1$, $K_D = 0$). However, this does not reduce frequency drop the most. The optimal configuration for reducing frequency drop is actually something close to $K_{SDM} = 0.5$ and $K_D = 0.5$. Put simply, faster contribution is not better.

This characteristic can likely be traced back to the governors of the residual grid, since the frequency is the control measure, which is altered. The causality however is hard to pinpoint, as frequency (frequency balance), governor control (grid power) and wind turbine inertia response are mutually coupled. What can be learnt from this test however, is that our inherent knowledge about power system behaviour may need to be challenged. Classic generation is often characterised by its own contribution to the grid and its dynamic responses, but facing a new generation, such as wind power, the interaction with the grid is equally, or more, important. The auxiliary control must then be regarded as a method for improving system interaction, rather than local contribution. The lagging wind turbine inertia response facilitates an effective primary regulation of residual grid by providing inertia reserves at the right time, but also demanding accelerating power at the right time.

7.3 HVDC-connection vs. Direct Connection

Revisiting section 6.1, all results yield that the impact of HVDC connection is marginal when opting for the current control design. The bode plot in figure 6.4 examine the offshore frequency response with onshore frequency as control variable shows efficient regulation for frequencies lower than 2 Hz. With frequency responses ranging from 1 Hz and lower, the regulation can be regarded more than adequate. Overlaying the frequency responses with and without HVDC-link included supports the arguments, figure 7.1. Revisiting the linearisation results from section 6.2.1 and 6.2.2, the dominant poles is summarised in table 7.2. The poles is marginally altered when introducing the HVDC-link, and as observed in figure 7.1 the frequency is slightly lower with HVDC-connection.

Article [7] describes a control strategy of turbine DC-voltage where frequency support is achieved by the energy release discussed in section 2.3.3. This has not been tested, but the capacitance of the HVDC-link would be an equivalent energy storage. Even though the HVDC-voltage is regulated and does release energy, there is no indication of any noticeable contribution, referring to figure 7.1.

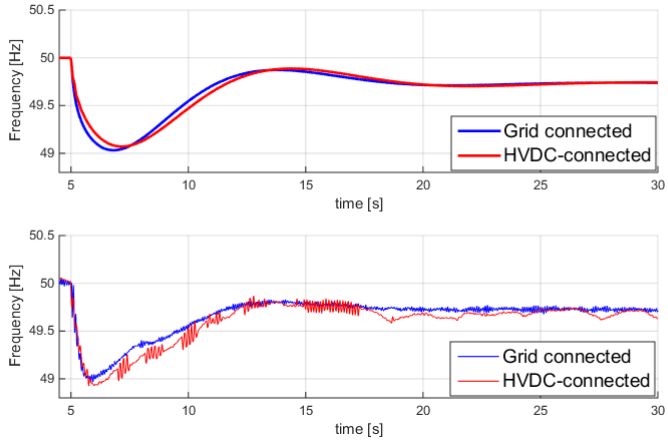

Figure 7.1: Onshore frequency response following a load disturbance. Auxiliary controls (SDM and WTS) implemented for inertia support from wind turbines. Over: Simulation Under: Laboratory

Table 7.2: Dominant poles observed as oscillations in frequency response plots with load as control variable with grid connected turbine (HVDC-link excluded).

Auxiliary Control	**Complex Pole**	**Natural Frequency,** ω_0	**Damping,** ζ	**Damped Frequency,** $\omega_d = \omega_0\sqrt{1-\zeta^2}$	**Oscillation Period** $t = \frac{2\pi}{\omega_d}$
No	$-0.481 \pm j1.07$	1.18 rad/s	0.408	0.97 rad/s	6.47 s
SDM, grid	$-0.210 \pm j0.6$	0.635 rad/s	0.33	0.566 rad/s	11.1 s
SDM and WTS, grid	$-0.269 \pm j0.432$	0.509 rad/s	0.53	0.431 rad/s	14.56 s
SDM	$-0.177 \pm j0.559$	0.586 rad/s	0.303	0.558 rad/s	11.25 s
SDM and WTS	$-0.234 \pm j0.424$	0.484 rad/s	0.484	0.348 rad/s	14.83 s

The resonance presented and investigated in section 6.3 may be a source of trouble. It was introduced by the coupling of onshore frequency and HVDC-voltage. Due to the specific limitations related to the current laboratory set up (high resolution DC-voltage reference, PLL-error and long computational time), this may be an non issue for other applications. The simulation model revealed a likely source for the resonance, but since there are also some limitations to the simulation model, this theory must still be regarded as speculations. The proposed solution - phase compensators in the DC-regulation - did however provide a degree of improvement, supporting the theory.

7.4 Wind Turbine Speed-Power Characteristics

Until this point it has been assumed that the mechanical input power to the wind turbine has been constant. Appendix B present the data associated with a turbine and calculations on aerodynamic behaviour, with respect to rotational speed is made. To summarise, at low wind speeds the wind turbine operate at a rotational speed and pitch to maximize power. When nominal power is reached, the rotational speed and pitch is controlled to maintain nominal power. When a wind turbine is controlled for inertia response, the change of rotational speed will shift the wind turbine from its nominal operation. If the shifted operating point result in significantly lower power output, the wind turbine inertia response would work opposite of its purpose.

Assuming that the wind turbine is operating at nominal rotational speed. From earlier results, a 20 *rpm* speed drop was observed. With a nominal speed of 500 *rpm*, this equals 0.04 *p.u.*. Using the data from figure B.5, the change in mechanical power is given by figure 7.2. For any operating point, a 20 *rpm* speed drop does not reduce power more than 0.01 *p.u.*. At high wind speeds, the power production is even increased, contributing positively. It can safely be assumed that an inertia response does not drastically reduce ability of the wind turbines to contribute inertia support. How an increased power production in combination of inertia energy release impact system dynamics, should however be evaluated.

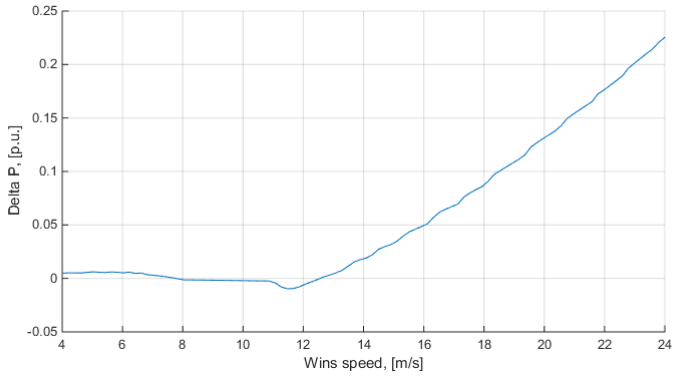

Figure 7.2: Change of mechanical power as function of wind speed, given a 0.04 *p.u* rotational speed drop.

7.5 Deviations

The main deviation between laboratory- and simulation models is the mode observed during the first half period of the onshore frequency response. Some additional results are given in appendix A. Figure A.5 highlight the mode. Figure A.6 shows that the auxiliary control act as expected in both models, and is ruled out as the origin. Also, by the validations from C, the speed- and voltage controllers act as desired. It must therefore be result of electric or mechanic characteristics not included in the simulation model. Two possible explanations may be:

- Voltage dependency: There voltage regulation of the wind turbine generator is not included in the simulation model. It was showed in appendix C that voltage dependency of the laboratory model could cause deviations.
- Motor- to generator-mode: Since the wind generator is actually run as a motor with no mechanical load, the power demand is very low (friction). When an inertia response is invoked, the power flow may reverse, and by such the go from motor to generator. Flux- and rotor angle dependency may then play a bigger role, invoking the discussed mode.

7.6 Real World Application

Since the laboratory has very low inertia - no wind turbine blades, water wheels etc. - the frequency response is very dramatic. However, by the arguments made in the introduction of chapter 6, the distribution of inertia is representative for a real world power system. By the inverse proportionality of inertia and acceleration, the qualitative effect of the inertia responses are transferable.

The simulation model has proven to be accurate accurate when it comes to nadir and sustained oscillations. In appendix A there is presented a system with foundation in an actual wind farm off the coast of Germany. The system is assumed to be 30 % wind power, similar to the laboratory. With higher inertia, the frequency deviations is more realistic, ranging up to half a hertz at worst. Introduction of inertia response from the wind turbines reduce the nadir by about a third when auxiliary controls is implemented (SDM and WTS), even with the gain $K_T = 0.5$, which is less than earlier testing. The speed response with SDM- and WTS-control is about 0.0067 $p.u.$, where as the grid frequency drops by about 0.007 $p.u.$.

Chapter 8

Conclusion

The main objective of this thesis - improving the dynamic frequency behaviour of the system - has been achieved and demonstrated. The results does portrait this quite clearly, without needing further explaining. The way to achieve this on the other hand, has greatly contributed in fulfilling the secondary objectives - highlighting VSC-control flexibility and gaining understanding of the interaction between the classic power system and converter interfaced generation. There are especially two points witch should be mentioned - how a phase lagged wind turbine inertia response improves system performance greatly, and how frequency mirroring over HVDC-link affected the system performance.

That a lagged wind turbine response improves the overall performance of the system is only logical if the general power system understanding is put to the test. The critical role of the governors sets the premise. The wind turbine speed response increase the total inertia of the system, but does not contribute in regulating it. Higher inertia makes the system more robust, but an otherwise unaltered primary regulation will struggle more to reach steady state frequency. As discussed in both the design and tuning section of the WTS-control, the governors are responsible for providing power in reaccelerating the wind turbines, and letting this acceleration happen at the same time as the governor mechanical power production is overshooting will improve the damping.

By confirming that a lagging wind turbine inertia response improves the damping of the system frequency, some conclusions can be made regarding the HVDC-connection. The inclusion of a HVDC-link did initially arise a natural question, whether this addition creates substantial delays. Since this thesis designed a inertia support strategy where regulation quickness is not all that important, this discussion is no longer relevant. However, since it is desired for the wind turbine response to be delayed, the auxiliary HVDC-control can be made purposely slower, and tune the wind turbine auxiliary control according to this. This makes it far more easy to maintain component ratings, as quick regulation of DC-voltage tend to draw high currents. This is a strength in the design, and allow the controller to be robust.

Some additional system characteristics was found when investigating the resonance invoked by the coupling of onshore grid frequency and HVDC-voltage. Since the frequency time variation is determined by power balance, there are potential fall pits when coupling the frequency to the VSC-controller, which main control objective is power flow. However, as the resonance likely was triggered due to system flaws - high sampling time, high HVDC-voltage reference resolution and PLL-error - this problem may be irrelevant if the system where to be realised. Even so, evidence suggested that the resonance was sustained by the control system, and some actions were needed. A simple phase compensator was designed, and the results improved.

Chapter 9

Further Work

Improve Modelling

The resonance found during testing was traced back to some unfortunate laboratory characteristics. Making some improvements to the software and/or hardware would enable the DC-voltage reference to be finer and ensure better PLL-behavior, possibly removing the resonance. However, this is minor updates that in practice doesn't alter the system in any fundamental way.

It was indicated that operating the wind turbine laboratory equivalent as a motor, rather than a generator, may not have been a justified simplification by the mode observed and then discussed in 7.5. It is anyway advantageous for the model to include wind turbines as a power source, not just an source of inertia.

A simulation model with the inclusion of electric properties may improve system understanding. Also, if the wind power plant where to be included in a bigger power system, the chosen model would likely be too simple. Large system that include multiple bus bars, where the power flow plays a vital role, a lack of voltage modelling would not suffice.

Voltage Regulation

It has been proven that the flexibility of VSCs allow for full converter wind turbines to provide system services much more efficiently than older wind power topologies. The VSC was presented with independent control of active- and reactive power as one of the major advantages. This could, and should, be utilised to a greater degree, as voltage regulation largely is reactive power regulation. Designing auxiliary VSC-control for voltage stabilisation, in addition to inertia control, would further allow higher share of wind power in the systems. Such a configuration would demand a more complex simulation model. The laboratory model on the other hand is configured for these kind of controllers.

Faults

A relevant study related to wind installation control would be AC- and DC-faults in the system. As the controllers have been tested under synchronous conditions, it is hard to predict how the system would react to disconnections or re-connections. Also, since DC-voltage is the power balance indicator on DC-side, short circuits in the DC-link would pose specific challenged for the control system. Voltage control would also be a specific challenge during faults, which further motivate expansion of simulation model and auxiliary controllers.

Multiterminal DC-grid

A possibility in future power systems is to design DC-grids with integrating offshore power production sites. Coordination of response is then the specific challenge in power flow control, and also in implementation of frequency support.

Collection Grid Coordination

As multiple turbines are to interact simultaneously, an investigation of system response time, resonances or other could be carried out.

Other Configurations

Battery storage, additional capacitors or other configurations could theoretically further enhance frequency stability support. Energy storage could prove to be a viable solution in combination with constant power production configurations and/or DC-voltage support. With rapid development in battery technology, power and capacity render batteries relevant for high voltage applications.

Bibliography

[1] ENTSO-E, *Network Code for Requirements for Grid Connection Applicable to all Generators*, 8 March 2013.

[2] ENTSO-E, *Network Code on HVDC Connections*, 30 April 2014.

[3] DTU 10 MW reference wind turbine, Data Provided by Karl Merz, Sintef Energy, `http://www.vindenergi.dtu.dk/`

[4] ZHU Jiebei, BOOTH Campbell D., ADAM Grain P., ROSCOE Andrew J. , *Inertia Emulation Control of VSC-HVDC Transmission System*, The International Conference on Advanced Power System Automation and Protection, 2011.

[5] L. Wu, D.G. Infield, J. Feuchtwang, *FREQUENCY SUPPORT FROM WIND PLANT TO POWER SYSTEMS*, Sustainable Power Generation and Supply, International Conference, SUPERGEN 2012.

[6] O. Anaya-Lara, F. M. Hughest, N. Jenkins, G. Strbactt , *Contribution of DFIG-based wind farms to power system short-term frequency regulation*, Generation, Transmission and Distribution, IEE Proceedings-(Volume:153 , Issue: 2), March 2006.

[7] Jiebei Zhu, Helge Urdal, Derek Young, *Synthetic Inertia Control Strategy for Double-fed Induction Generator Wind Turbine Generators Using Energy from DC Capacitor*, Wind Integration workshop, 2013

[8] Machowski, Bialek and Bumbi, *Power System Dynamic Stability and Control*, Wiley

[9] Bahrman, M.P. ; Johnson, B.K., *The ABCs of HVDC transmission technologies*. Power and Energy Magazine, IEEE (Volume:5 , Issue: 2), page 32-44, 12 march 2007

[10] Mohan, Undeland and Robbins, *Power Electronics*, MNPERE, Inc., ISBN 0-9715292-0-5, 2001

[11] Hadi Saadat, *Power System Analysis*, Third Edition, PSA Publishing, 2010.

[12] NED MOHAN, *Advances Electric Drives*. Power and Energy Magazine, John Wiley & Sons, Inc., ISBN 978-1-118-07481-7, 2012

[13] NED MOHAN, *Electric Machines and Drives: A first Course*, MNPERE, Inc., ISBN 0-9715292-0-5, 2001

[14] Chandra Bajracharya, *Control of VSC-HVDC for wind power*. Master Thesis, NTNU, 18. jun 2008.

[15] Temesgen Mulugeta Haileselassie, *Control, Dynamics and Operation of Multi-terminal VSC-HVDC Transmission Systems*, NORPIE/2008, PhD Thesis, NTNU, December 2012.

[16] Hanne Støylen, *Laboratory Demonstration of Provision of Primary Frequency Control Services from HVDC-VSC Connected Wind Farms*, Master Thesis, NTNU, 10. jun 2014.

[17] F. Mayouf (Adjeroud), F. Djahli and A. Mayouf, *Study of Excitation and Governor Power System Stabilizers Effect on the Stability Enhancement of a Single Machine Infinte-Bus Power System*, Environment and Electrical Engineering (EEEIC), 2013 12th International Conference, 5-8 May 2013, IEEE.

[18] Ahmed A. Ba-muqabel, Dr.Mohammad A. Abido, *Review of Conventional Power System Stabilizer Design Methods*, Generation, GCC Conference (GCC), 2006 IEEE.

[19] C. Tang, M. Pathmanathan, W.L. Soong and N. Ertugrul, *Effects of Inertia on Dynamic Performance of Wind Turbines*, Power Engineering Conference, 2008. AUPEC '08. Australasian Universities, 14-17 Dec. 2008.

[20] National Instruments: LabView, Home page, `http://www.ni.com/labview/`

[21] Astrid Petterteig, *Specification of equipment for the small hydro generator model for the Sintef/NTNU-renewable energy laboratory*, technical report, SINTEF Energy Research, 2008

[22] Astrid Petterteig, *General description of MV distribuition network model for the Sintef/NTNU-renewable energy laboratory*, technical report, SINTEF Energy Research, 2008

[23] Astrid Petterteig, *Distribution network laboratory model*, technical report, SINTEF Energy Research ,2011

[24] Kjell Ljøkelsøy, *60 kVA laboratory converter unit, documentation. Technical report*, SINTEF Energy Reserch memo, 2010.

[25] Kjell Ljøkelsøy, *Control system for a three phase grid connected converter. Technical report*, SINTEF Energy Reserch memo, 2014.

[26] Hansen, M.O.L.; Aerodynamics of Wind Turbines; Second Edition, Earthscan, 2008

Appendix A

Additional Results

A.1 Adjusted Wind Turbine Speed Response

The gain of the wind turbine auxiliary control, K_T, is adjusted so that the speed response is 20 rpm. All parameters is found in table A.1. The parameters is referred to figures 4.4, 4.5and 4.9.

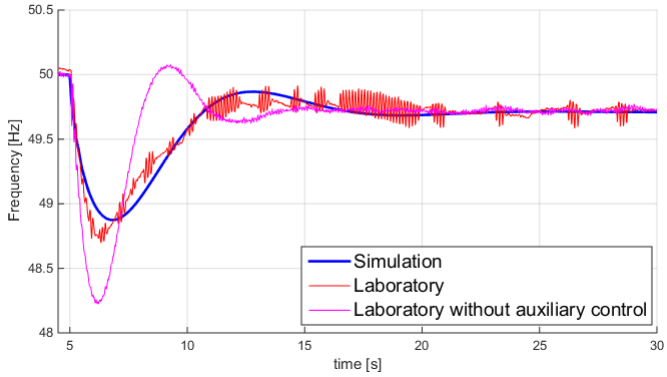

Figure A.1: Frequency response of onshore grid imposing a 0.0588 p.u. load step in laboratory and simulation with implemented SDM- and WTS-control in HVDC-connected FCWT.

Table A.1: Auxiliary control parameters of full system configuration with wind turbine speed response maintained.

Parameter	**Value**
HVDC-voltage Control	
K_V	0.5
$T_{V,filt}$	0.01 s
Offshore Frequency Control	
K_f	2
$T_{f,filt}$	0.01 s
Wind Turbine Speed Control	
$T_{T,filt}$	0.01 s
K_{SDM}	1
$T_{hp,T}$	10 s
K_D	1.5
$T_{w,T}$	10 s
K_T	0.66
Transfer function	$\frac{1}{1+3s}$

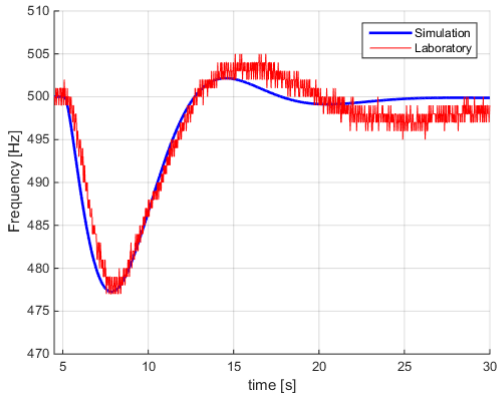

Figure A.2: Wind turbine speed response when imposing a 0.0588 p.u. load step. Results from laboratory and simulation with implemented SDM- and WTS-control in FCWT connected by HVDC to grid.

A.2 Real World Case Study

The real world case is gathered from the wind farm Borwind 1, situated on the coast of Germany. It uses HVDC Light technology by ABB. Parameters not available are estimated. The capacitance of the converters are the most uncertain parameter, but are estimated to produce a converter time constant ($\tau = \frac{\frac{1}{2}CV_n^2}{P_n}$) of $5 - 10\ ms$. The relevant parameters are given by table A.2. The auxiliary control parameters are given by table A.3.

Table A.2: Technical data for Borwind 1 wind farm.

Parameter	**Value**
Grid	
Inertia constant, H_{eq}	$5\ s$
Droop constant, ρ	$4\ \%$
Nominal power, S_n	$400\ MW$
Frequency, $f_{onshore}$	$50\ Hz$
HVDC	
Nominal power, $S_{HVDC,n}$	$400\ MW$
Nominal voltage, $U_{HVDC,n}$	$\pm 150\ kV$
Time constant, $\tau_{HVDC} = \frac{\frac{1}{2}CU_{HVDC}^2}{S_n}$	$10ms/terminal$ $(C_{VSC} = 444\ \mu F)$
XLPE submarine cable	
Length, l	$125\ km$
Area, A	$1200\ mm^2$
Capacitance, C_{XLPE}	$0.2\ \mu F/km\ =\ 25\ \mu F$ $(\tau_{XLPE} = 1.13\ ms)$
Frequency, $f_{offshore}$	$50Hz$
Wind Turbine	
Nominal power, $S_{WT,n}$	$2\ MW$
Nominal DC-voltage, U_WT, n	$690\ V$
Time constant, $\tau_{WTC} = \frac{\frac{1}{2}CU_{WT}^2}{S_n}$	$10\ ms$ $(C_{VSC} = 84\ mF)$
Inertia constant, H_{WT}	$9\ s$
Nominal rotational speed, $\omega_{WT,n}$	$2\ rad/s$
Load	
Nominal load, P_L	$800\ MW$

Figure A.3 is the simulated results of the frequency response from a $0.0588 p.u.$ load step. The WTS was adjusted after observing the dominant oscillation when SDM-control was implemented. Since the inertia of the system is higher, the oscillations are slower, and the WTS-control should therefore be effective at a lower frequency.

Table A.3: Auxiliary control parameters of real world configuration, referred to figure 4.4, 4.5 and 4.9.

Parameter	**Value**
HVDC-voltage Control	
K_V	0.5
$T_{V,filt}$	0.01 s
Offshore Frequency Control	
K_f	2
$T_{f,filt}$	0.01 s
Wind Turbine Speed Control	
$T_{T,filt}$	0.01 s
K_{SDM}	1
$T_{hp,T}$	50 s
K_D	1.5
$T_{w,T}$	30 s
K_T	0.5
Transfer function	$\frac{1}{1+3s}$

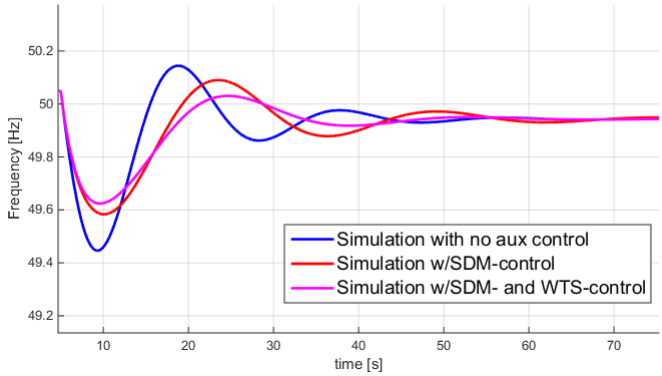

Figure A.3: Frequency response of onshore grid imposing a 0.0588 p.u. load step by simulation of the real world configuration.

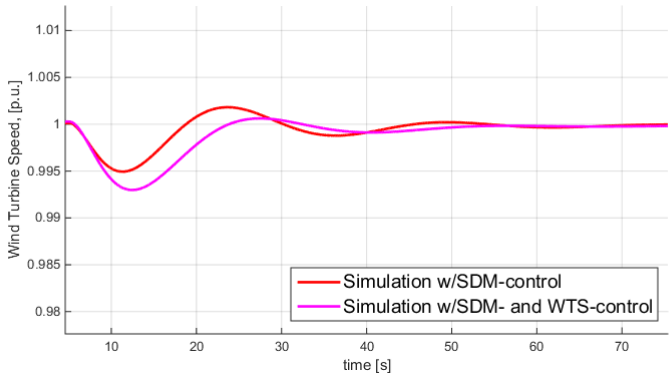

Figure A.4: Wind turbine speed response imposing a 0.0588 p.u. load step onshore. Results from simulation of the real world configuration.

A.3 Deviation

Figures to support discussion in 7.5. The responses from figure A.6 are almost indistinguishable. Figure A.5 is the onshore frequency response wihtout HVDC-link. The HVDC-link is excluded due to the earlier mentioned resonance which makes the deviation less visible.

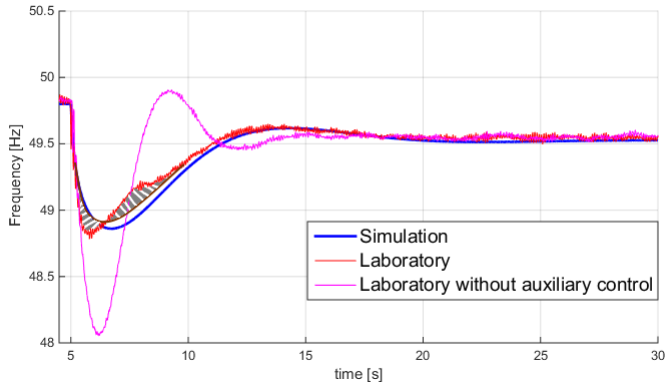

Figure A.5: Onshore frequency response with highlight of the relevant deviation between laboratory and simulations. Deviation is marked in gray. Grid connected turbines with SDM- and WTS-control.

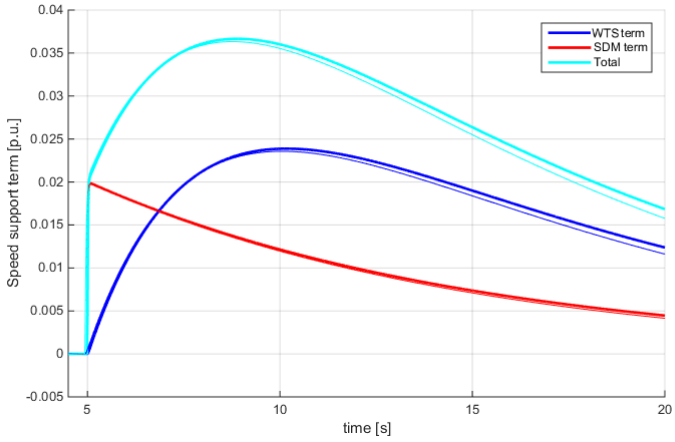

Figure A.6: Wind turbine auxiliary control response imposing a fictitious offshore frequency step. Results from simulation (thick) and laboratory (thin).

Appendix B

Wind Turbine Aerodynamics

This section revisits the statement made in 2.3 regarding the mechanical input power to a wind turbine being constant at varying generator rotational speed. In order to make a proper evaluation, the basics of aerodynamic behaviour of wind turbines are presented.

B.1 Aerodynamic Basics

The power of a wind turbine is dependent on blade wind efficiency and wind speed. The density of the air produces a thrust on the blades, causing it to rotate. The high velocity of the blades causes turbulence and vortexes at the tips of the blade rendering most common fluid mechanic simplifications to be invalid. Heavy simulation tools is needed in order to precisely estimating the power. Simulations and experiments show that the maximum power a wind turbine can extract from a air flow is 59.3%. This is called the Betz limit. Details on these topics can be found in [26].

For the purpose of this tesis, a reference turbine has been chosen. The turbine chosen is the 10 MW reference wind turbine developed by "Danske Tekniske Universitet" [3].

The power of the wind turbine is expressed by the following equation.

$$P = \frac{1}{2}\rho A V_{wind}^3 C_p(\lambda, \beta) \tag{B.1}$$

$$\lambda = \frac{\omega R}{v} \tag{B.2}$$

The power is dependent on the cube of wind speed and the blade efficiency, expressed by the power coefficient C_p, which is a dimensionless quantity. λ is the ratio between tip speed and wind speed and β the pitching angle of the blades. The DTU-turbine has been described as a function of these and figure B.2 shows the characteristics.

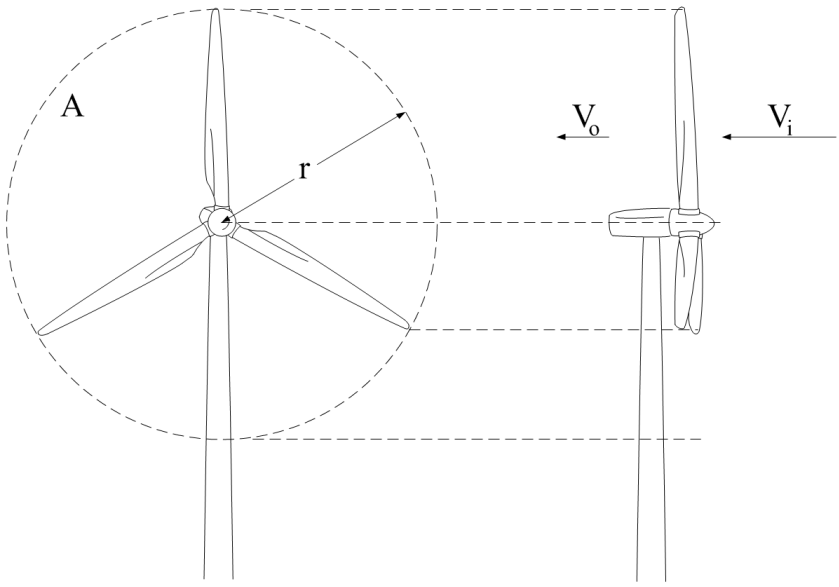

Figure B.1: 3-blade horizontal wind turbine

The isocurves indicates constant power. The line across them is the characteristics chosen for this specific wind turbine. These are chosen in order to maximize the output power in low wind conditions and to maintain it in high wind conditions. The wind speed is indicated along the line. The wind speed-power-characteristics along the line is given by figure B.3. Since the line is estimated by using linear interpolation between known speed-power setpoints, the curve has some irregularities along the constant nominal power region, but sufficient to describe the behaviour.

For this particular wind turbine, the cut in speed is $4m/s$. This is the wind speed at which the turbine starts producing power. The power increases by the cube of wind speed, until it reaches nominal power of $1p.u.$. The pitching and rotational speed is then controlled in order to operate at nominal power until the cut off speed of $25m/s$.

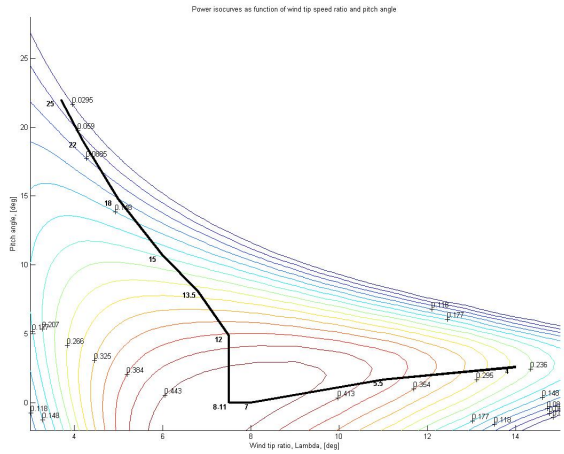

Figure B.2: Power coefficient as function of λ and β

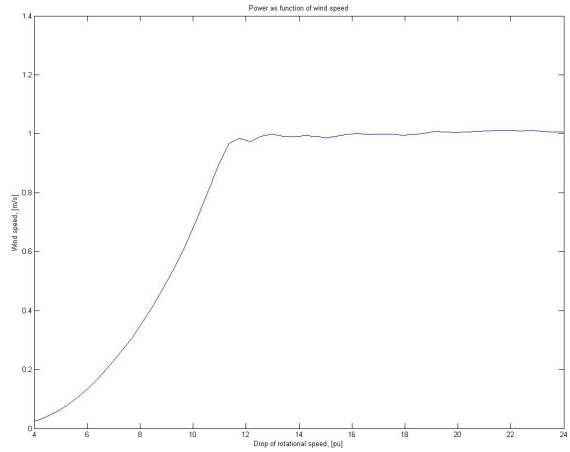

Figure B.3: Power as function of wind speed

B.2 Wind Power and Stability Properties

The motivation of including a section on wind turbine behaviour was to investigate the effect of rotational speed drops on output power. As shown, λ is proportional to rotational speed. A drop in rotational speed, as desired in inertial responses, forces λ to drop. The new operation set point will in turn result in a new mechanical power input. Figure B.4 indicates how λ shifts when a $0.2p.u.$ drop of rotational speed is introduced. The power is then plotted as function of wind speed and rotational speed drop in order to illustrate the effect of deviating from nominal values, figure B.5.

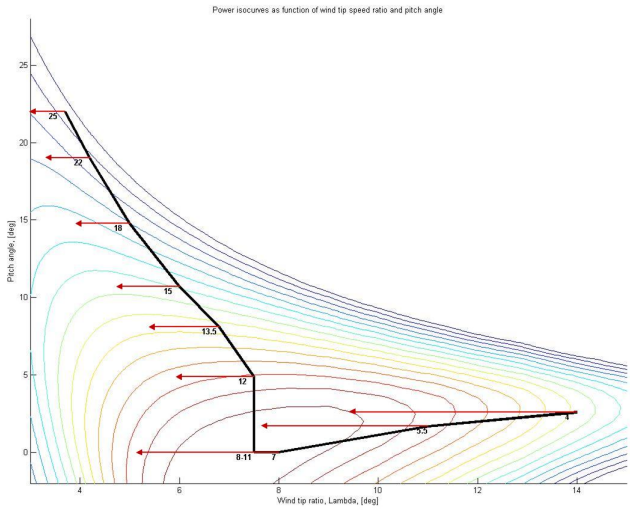

Figure B.4: Power coefficient as function of λ and β with λ-shifting indicated.

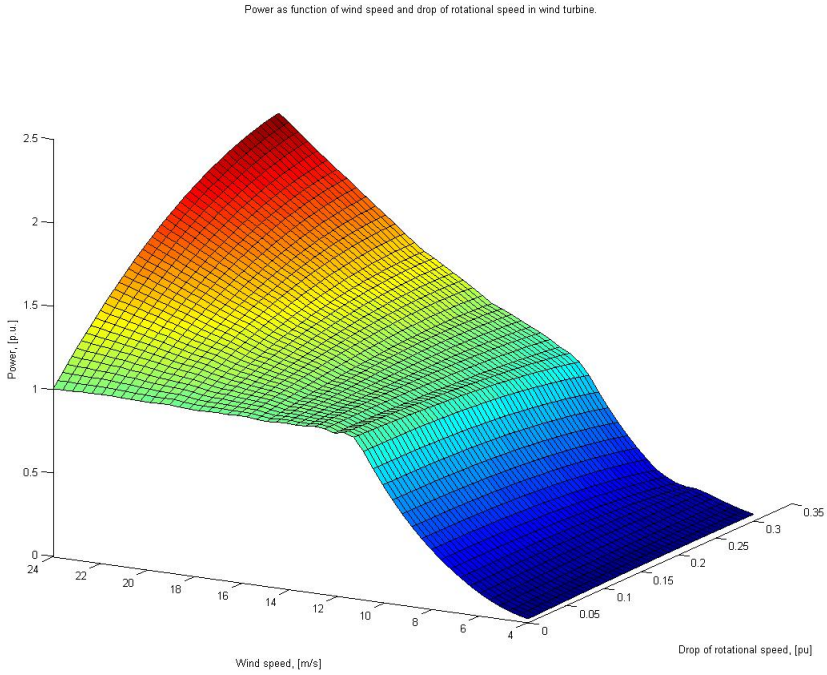

Figure B.5: Power as function of wind speed and rotational speed drop.

Appendix C

Model Validations

C.1 Onshore Grid

The unregulated system is characterised by the swing equation (2.1). Evaluating the block diagram from figure 5.1, the system equation is a pure integrating term, producing a 90° phase lag and a $-20\ dB$ gain per decade, illustrated in the bode plot in figure C.2. It should be noted that the inertia constant is the decisive parameter in determining the absolute value of the system gain. This is consistent with the conclusion made in chapter 2, where the rate of change in frequency is dependent on the system inertia.

The simplified power system and regulation has been discussed in chapter 5.1. To summarise, the electrical transients are neglected as the inertial response are of interest. It is assumed that the system is rotor angle stable. By introducing an acting droop governor to the system, the power production is regulated in order to compensate for power imbalances. Figure C.1 shows the onshore grid frequency response imposing a load step. The actual governor PI-control settings in the lab are $K = 1$ and $T = 0.8\ s$. Not all parameters of the laboratory governor control is known, and it is more complex than the simulation model governor. By modifying the simulation model PI-control parameters, the response is fitted to the laboratory results. Note that all further references to governor PI settings are referred to the laboratory settings. The bode plot in figure C.2 shows the regulated system with load power as control variable and grid frequency as output variable. The governor settings are unchanged until otherwise specified.

As expected, low frequencies are perfectly regulated as governor action is sufficiently quick to keep up, while high frequencies are suppressed by the inertia of the system. The gain at low frequencies are determined by the droop ($\rho = \frac{\Delta f}{\Delta P}$). With $\rho = \frac{1}{9.93} = 0.101$ the amplitude at low frequency will have a gain of $20log(\rho) = -19.93$. It should be noted that the governor is purposely tuned non-ideally for the system to produce oscillations. Investigating the Pole-Zero-diagram, figure C.3 shows a pole at $1.12\ rad/s$. For an underdamped system the damped frequency can be found by the expression $\omega_d = \omega_0\sqrt{1-\zeta^2}$, where ω_0 is the natural frequency and ζ is the damping

coefficient. The damped frequency will in this case be 1.023 rad/s, which also can also be observed in figure C.1.

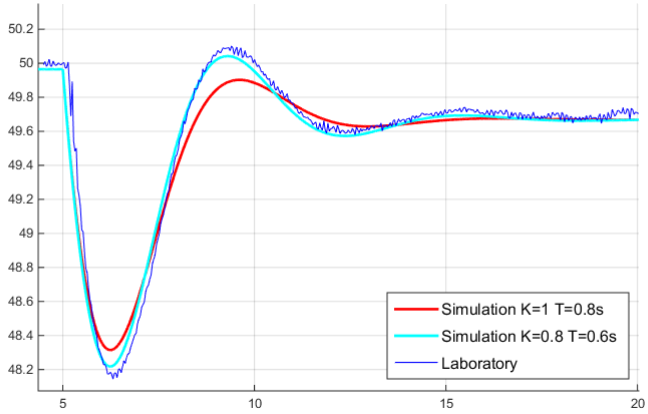

Figure C.1: Frequency response imposing a load step of 0.0588 p.u.. Results from simulations with two different sets of control parameters, and laboratory

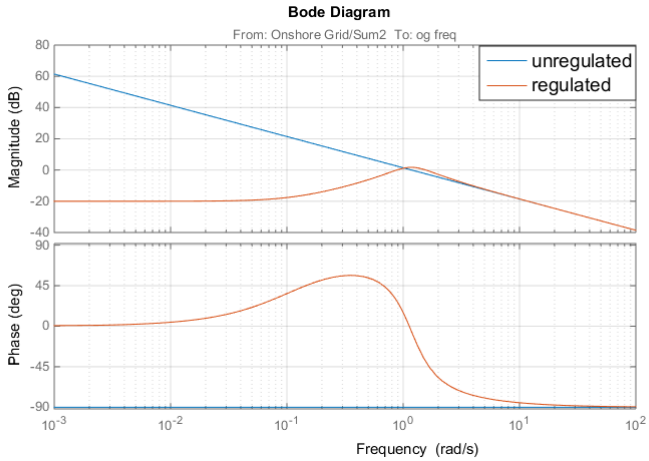

Figure C.2: Bode-plot of the unregulated and regulated onshore grid

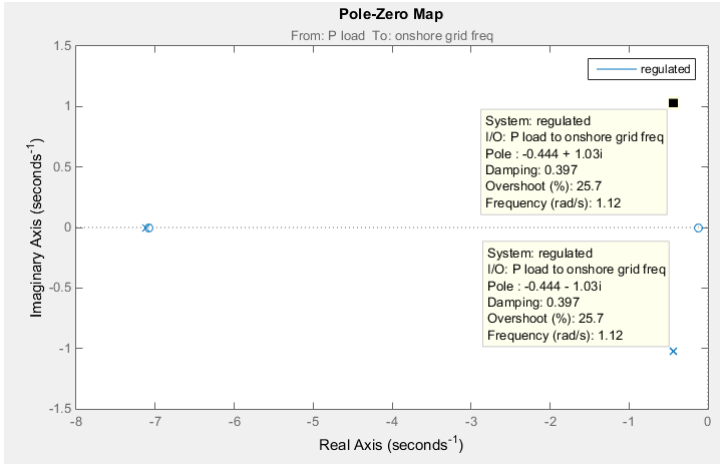

Figure C.3: Pole-Zero-plot regulated onshore grid

C.1.1 Effect of Load Step Size

The system is subjected to a load step disturbance. In order to further validate the model, different step sizes is imposed, and the frequency response is observed, figure C.4. With increasing load step, the deviation in the simulation model is greater. One simplification in the simulation model is that the load power is voltage invariant. The laboratory load is a pure resistance, and the load power is such a function of the voltage by the equation $P_L = \frac{U^2}{R}$. Plotting the voltage, figure C.5, the voltage drop is increasing for increasing step size. For $\Delta P = 0.053$ $p.u.$, the peak load deviation would be about 8%. Going back to figure C.4, this is hardly observable in onshore frequency response. When $\Delta P = 0.106$ $p.u.$ and $\Delta P = 0.159$ $p.u.$, the peak load deviation would be about 15% and 20% receptively, which makes for a noticeable margin of error in the simulated results. The load step disturbance is therefore kept at a minimum, but still realistic, $0.058 p.u.$ if otherwise is not specified.

C.1.2 Speed controller

The wind turbine equivalent is speed controlled with a reference given by the optimal rotational speed as a function of wind speed. The speed controller is tested to match the speed step response of the laboratory. Figure C.6 and C.7 shows the laboratory and simulation model response for two step sizes.

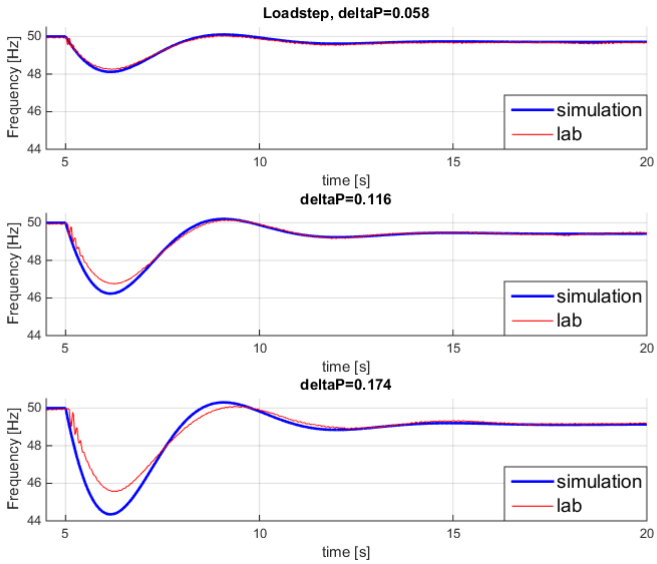

Figure C.4: Onshore frequency response when system is subjected to load disturbances of different magnitudes.

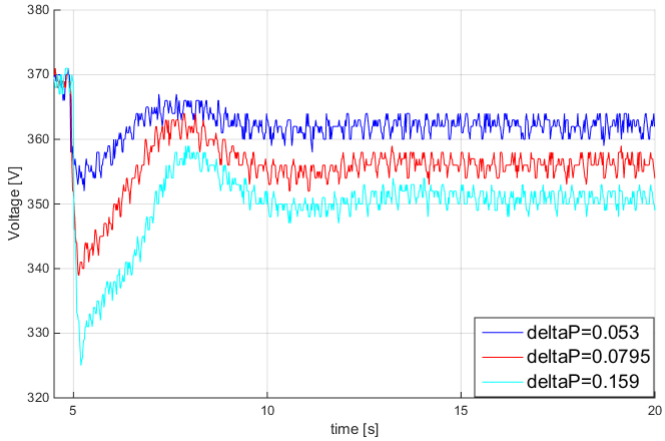

Figure C.5: Onshore voltage when system is subjected to load disturbances of different sizes.

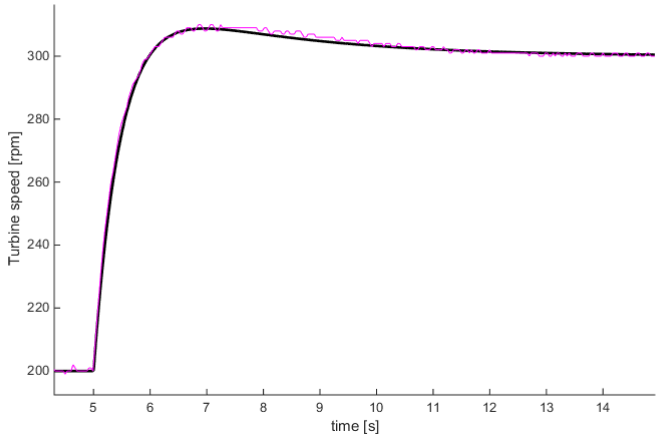

Figure C.6: Speed step 200 to 300 rpm

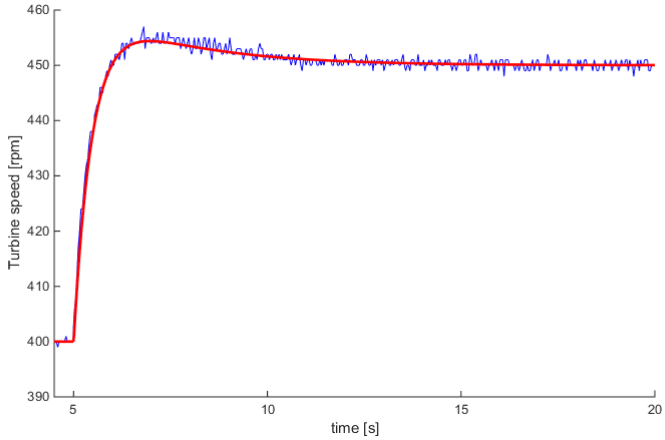

Figure C.7: Speed step 400 to 450 rpm

C.1.3 Voltage controller

Similarly as for speed control, the DC-voltage control is tested in the laboratory and compared to simulation results. Figure C.8 shows good correlation between laboratory and simulation.

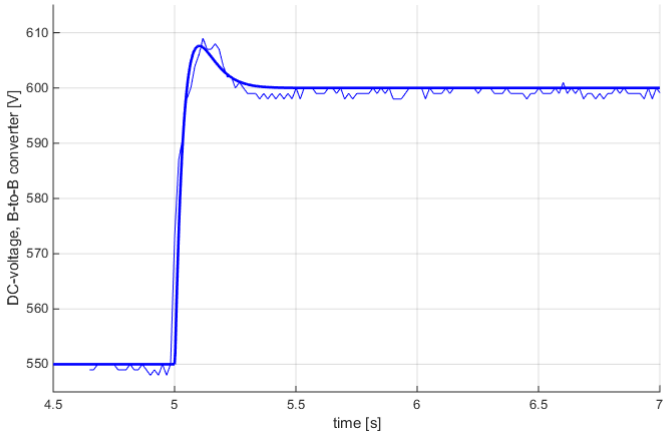

Figure C.8: Voltage step, 550 to 600 V

C.2 Phase Lock Loop Testing

The phase lock loop is essential in producing the switching schemes for the converters. Since he offshore grid is inertia free, the frequency could potentially be changed very quickly. The PLLs should be tested isolated in case they pose a delay or have problems following the frequency changes all together.

Figure C.9 show the laboratory set up for testing the PLLs. Since all the converters are implemented with the same software, it is assumed that all PLLs behave alike. A synthesized AC-grid is produced by converter C, and the frequency reference of said converter is changed by a step. The frequency measurement is made by converter E-1. Figure C.10 shows the frequency reference, the measured frequency, and a response approximated in by a second order transfer function. The transfer function is added to the simulation model to include PLL behaviour.

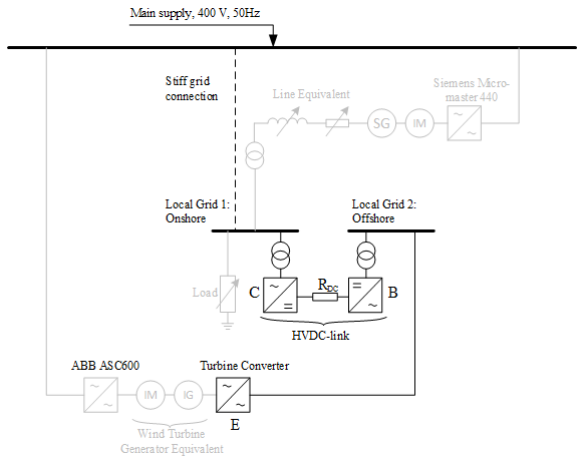

Figure C.9: Laboratory setup for testing Phase Lock Loops by a offshore frequency step produced by converter C and measurement from converter E-1.

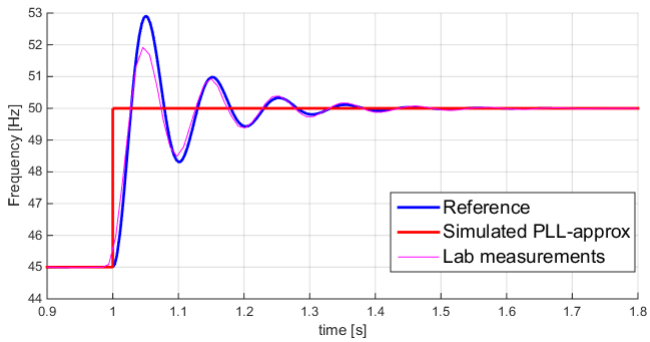

Figure C.10: Subjecting the PLL-measurement to a frequency step.

Appendix D

Simulation Model

The simulation model is built with foundation in equations derived in chapter 3 and 4. That is, swing equation for the distribution grid and wind turbine, and DC-capacitance voltage balance for DC-links. Auxiliary control is implemented directly from figures also found in chapter 4. Note that there are manual switches to choose fixed- or a step reference, where the step references are included for individual testing of controller, i.e. tuning of the DC-voltage regulators.

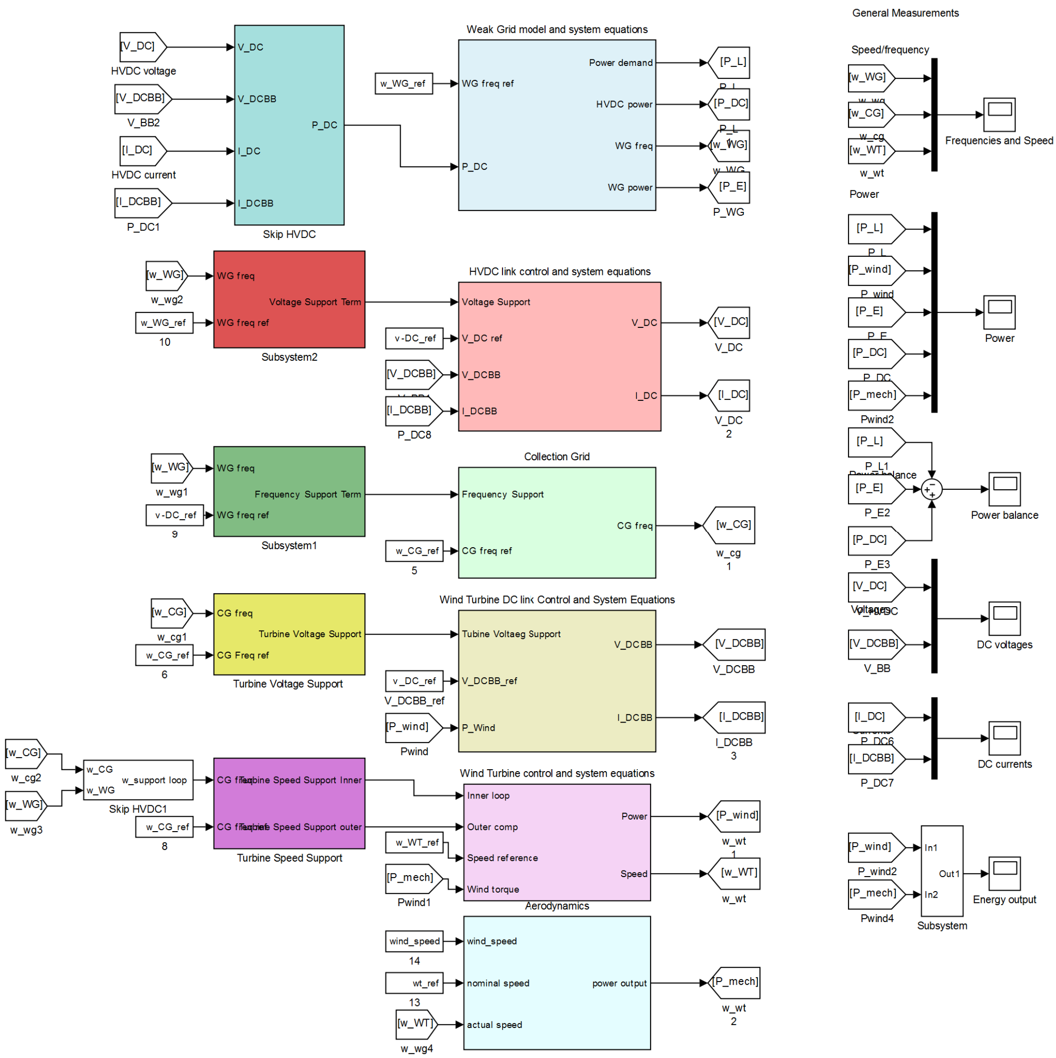
General Measurements
Speed/frequency
Frequencies and Speed
Power
Power balance
DC voltages
DC currents
Energy output
Weak Grid model and system equations
Skip HVDC
HVDC link control and system equations
Subsystem2
Collection Grid
Subsystem1
Wind Turbine DC linc Control and System Equations
Turbine Voltage Support
Wind Turbine control and system equations
Turbine Speed Support
Aerodynamics
Skip HVDC1
Subsystem
HVDC voltage
HVDC current
Voltage Support Term
Frequency Support Term
Turbine Voltaeg Support
Inner loop
Outer comp
Speed reference
Wind torque
wind_speed
nominal speed
actual speed
power output

D.1 Power System Model

Distribution grid

The droop control is implemented with a PI-controller. The power transmitted by the HVDC-link and load is added as disturbances post-regulator, pre-system. The system is the swing equation.

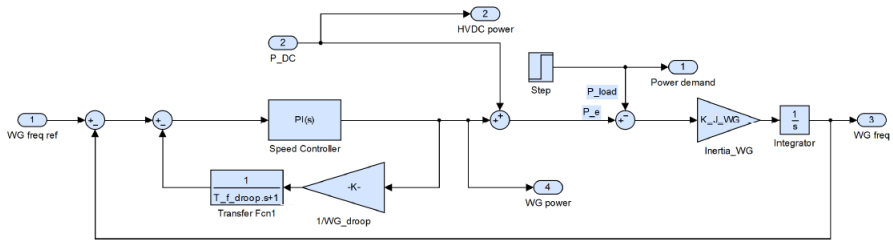

Figure D.1: Distribution grid Simulink model- governor regulation

HVDC-voltage Balance

Distribution grid converter controlling voltage with outer loop voltage control with a equivalent delay representing inner loop current control. The power injected is added as disturbance post-regulator and pre-system. The system is modelled by capacitor equation, and thus neglecting resistance.

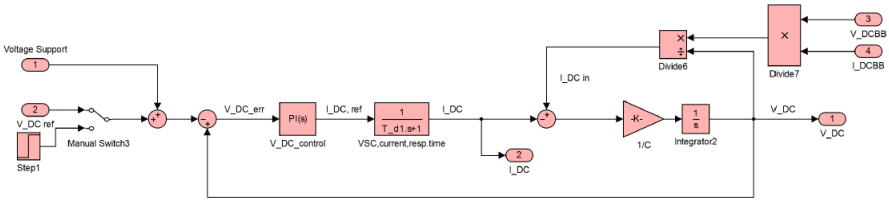

Figure D.2: HVDC-link SimuLink model - DC-voltage regulation

Offshore grid Frequency

Though not part of the power flow dynamics, the frequency is used for regulation purposes. Collection grid converter produces a voltage by the amplitude and frequency reference given.

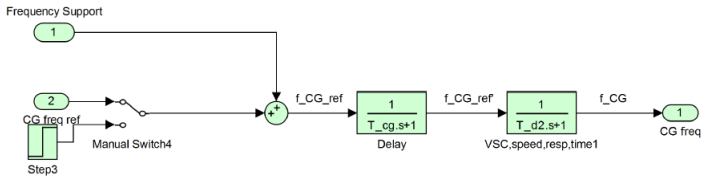

Figure D.3: Offshore grid SimuLink model - frequency regulation

Turbine Converter Voltage Balance

Same configuration as HVDC-link, wind turbine grid converter controlling voltage with outer loop voltage control with a equivalent delay representing inner loop current control. Power flow is indicated as disturbance post-regulator and pre-system. System modelled by capacitance equation.

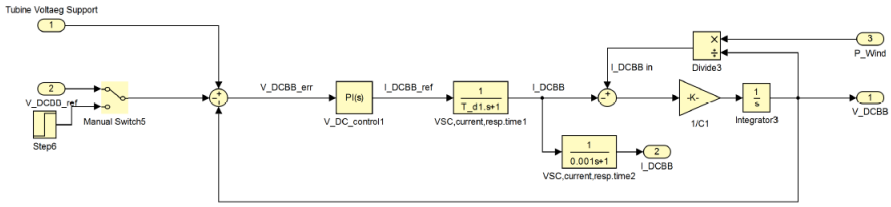

Figure D.4: Wind Turbine DC-link SimuLink model

Wind Turbine

Modelled by swing equation (torque balance), outer loop speed control and inner loop by torque control. Input from wind data is power, rather than torque, and is thus divided by speed.

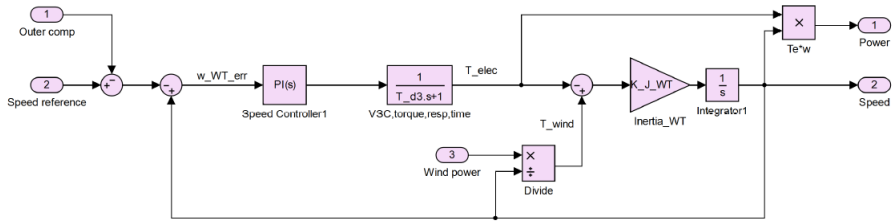

Figure D.5: Wind turbine electromechanical SimuLink model - speed regulated

Aerodynamic Data

Data given in chapter B provides tables by wind speed and speed deviation from nominal. Can be turned on and off.

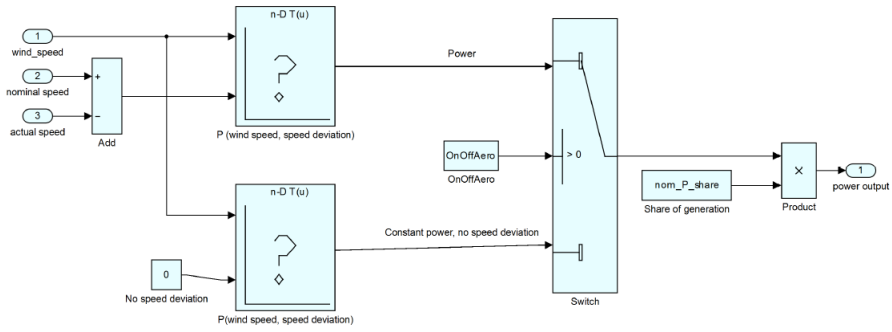

Figure D.6: SimuLink configuration for wind power-speed drop dependency

D.2 Auxiliary Control

Auxiliary HVDC-voltage Control

Auxiliary control with onshore grid frequency measurements and SDM-control og HVDC-voltage.

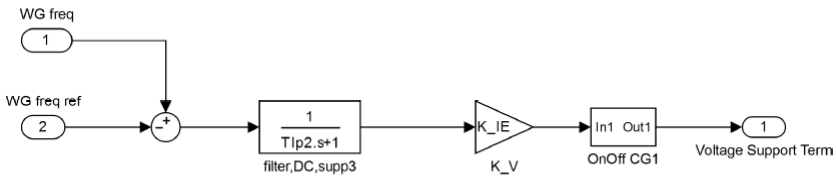

Figure D.7: Auxiliary HVDC-voltage control in Simulink

Auxiliary Offshore Frequency Control

Auxiliary control with HVDC-voltage measurements and SDM-control of offshore frequency.

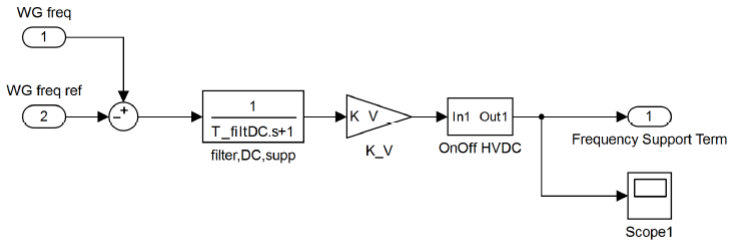

Figure D.8: Auxiliary offshore frequency control in Simulink

Auxiliary Wind Turbine Speed Control

Auxiliary control with offshore frequency measurement and SDM- and WTS-control.

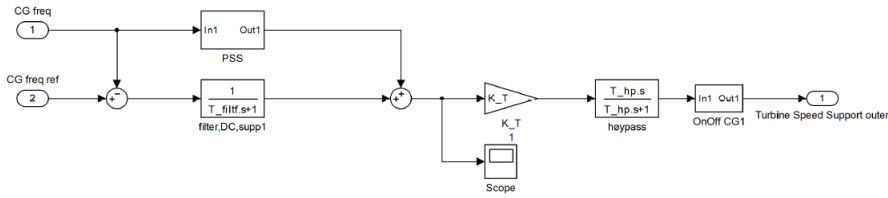

Figure D.9: Auxiliary wind turbine speed control in Simulink